

1 Title:

2 Fractionation of the methane isotopologues  $^{13}\text{CH}_4$ ,  $^{12}\text{CH}_3\text{D}$ , and  $^{13}\text{CH}_3\text{D}$  during aerobic oxidation of methane by  
3 *Methylococcus capsulatus* (Bath) [140 char w/ spaces]

4  
5 A manuscript revised for *Geochimica et Cosmochimica Acta* on 19 July 2016

6  
7 Authors and affiliations:

8 David T. Wang<sup>a,b,\*</sup>, Paula V. Welander<sup>c</sup>, and Shuhei Ono<sup>a</sup>

9 <sup>a</sup>Department of Earth, Atmospheric and Planetary Sciences, Massachusetts Institute of Technology, Cambridge, Massachusetts 02139, USA.

10 <sup>b</sup>Marine Chemistry and Geochemistry Department, Woods Hole Oceanographic Institution, Woods Hole, Massachusetts 02543, USA.

11 <sup>c</sup>Earth System Science Department, Stanford University, Stanford, California 94305, USA.

12  
13 \* To whom correspondence should be addressed:

14 David T. Wang  
15 Department of Earth, Atmospheric, and Planetary Sciences  
16 Massachusetts Institute of Technology  
17 77 Massachusetts Ave, Bldg. E25-645, Cambridge, MA 02139, USA.  
18 +1 (617) 324-3949  
19 dtw@mit.edu

20  
21  
22 *McB-13CH3D\_Revised\_v3b2.docx*

23

24

25

26 **Abstract [max 500 words, ideally 200-300]**

27 Aerobic oxidation of methane plays a major role in reducing the amount of methane emitted to the atmosphere  
28 from freshwater and marine settings. We cultured an aerobic methanotroph, *Methylococcus capsulatus* (Bath) at  
29 30 and 37 °C, and determined the relative abundance of  $^{12}\text{CH}_4$ ,  $^{13}\text{CH}_4$ ,  $^{12}\text{CH}_3\text{D}$ , and  $^{13}\text{CH}_3\text{D}$  (a doubly-substituted,  
30 or “clumped” isotopologue of methane) to characterize the clumped isotopologue effect associated with aerobic  
31 methane oxidation. In batch culture, the residual methane became enriched in  $^{13}\text{C}$  and D relative to starting  
32 methane, with D/H fractionation a factor of 9.14 ( $^{\text{D}}\epsilon/^{13}\epsilon$ ) larger than that of  $^{13}\text{C}/^{12}\text{C}$ . As oxidation progressed, the  
33  $\Delta^{13}\text{CH}_3\text{D}$  value (a measure of the excess in abundance of  $^{13}\text{CH}_3\text{D}$  relative to a random distribution of isotopes  
34 among isotopologues) of residual methane decreased. The isotopologue fractionation factor for  $^{13}\text{CH}_3\text{D}/^{12}\text{CH}_4$   
35 was found to closely approximate the product of the measured fractionation factors for  $^{13}\text{CH}_4/^{12}\text{CH}_4$  and  
36  $^{12}\text{CH}_3\text{D}/^{12}\text{CH}_4$  (i.e.,  $^{13}\text{C}/^{12}\text{C}$  and D/H). The results give insight into enzymatic reversibility in the aerobic methane  
37 oxidation pathway. Based on the experimental data, a mathematical model was developed to predict isotopologue  
38 signatures expected for methane in the environment that has been partially-oxidized by aerobic methanotrophy.  
39 Measurement of methane clumped isotopologue abundances can be used to distinguish between aerobic methane  
40 oxidation and alternative methane-cycling processes. [204 words]

41

42

## 1. INTRODUCTION

Methane is an important long lived (well-mixed) greenhouse gas whose atmospheric concentration has more than doubled (~720 ppb to >1800 ppb) since pre-industrial time (Wahlen, 1993; IPCC, 2013). Important sources of atmospheric methane include natural wetlands (up to one-third of emissions), agriculture (including paddy rice fields and ruminant animals), and fossil fuel usage (Bousquet et al., 2006; Dlugokencky et al., 2011). Methanogenic archaea are responsible for the majority of emissions, with thermogenic sources accounting for most of the remainder. The primary methane sink in the atmosphere is reaction with tropospheric hydroxyl radicals (OH). Despite rigorous bottom-up accounting and top-down estimates based on remote sensing data and high-frequency measurements, the flux of methane from sources and to sinks remains poorly constrained (e.g., Kirschke et al., 2013).

Emissions from natural and human-made wetlands and other aquatic environments account for nearly two-thirds of all methane sources, though substantial uncertainty is associated with source strength estimates (Kirschke et al., 2013). Methanotrophic processes consume over half of the methane produced in aquatic environments prior to emission into the atmosphere (Reeburgh, 2007). It is estimated that a large fraction of methane produced in freshwater sediments, as much as 90% at some sites (Oremland and Culbertson, 1992), is removed via the aerobic oxidation of methane. In addition, soil-dwelling aerobic methanotrophs are responsible for oxidation of a small fraction (~2%) of methane from the atmosphere (Kirschke et al., 2013). Furthermore, activity of methanotrophic bacteria with high affinity for atmospheric methane in Arctic soils has been reported (Lau et al., 2015). Thus, understanding the magnitude and dynamics of methanotrophic sinks is important for global methane cycle budgets and constraining inputs to climate simulations.

The bacterium *Methylococcus capsulatus* (Bath), an obligate aerobic methanotroph, is a model organism for studies of the genetics, physiology, and geomicrobiology of aerobic methane oxidation in sediments and water columns (Whittenbury et al., 1970; Bowman, 2014). This organism uses the enzymes soluble methane monooxygenase (sMMO) and particulate methane monooxygenase (pMMO) to oxidize methane to methanol, which is further oxidized to CO<sub>2</sub> as an end product (Hanson and Hanson, 1996). Carbon derived from methane can also be assimilated into cellular biomass. The overall reaction is thus described by the stoichiometry:



where C<sub>cell</sub> represents cellular carbon and *b* is the fraction of carbon assimilated into biomass.

In experiments with pure and enrichment cultures, microbes utilizing this pathway have been shown to generate large and correlated carbon (<sup>13</sup>C/<sup>12</sup>C) and hydrogen (D/H) isotope fractionations during aerobic methane oxidation (Coleman et al., 1981; Kinnaman et al., 2007; Powelson et al., 2007; Feisthauer et al., 2011). Measurements of <sup>13</sup>C/<sup>12</sup>C and D/H ratios in environmental methane samples can be used to assess whether they have experienced partial oxidation (Hornibrook et al., 1997; Chanton et al., 2005).

Recently, methods were developed to determine the abundance of multiply-substituted “clumped” isotopologues (e.g., <sup>13</sup>CH<sub>3</sub>D) in methane samples to sub-permille precision (Ono et al., 2014; Stolper et al., 2014b; Young et al., 2016). Measurements of the abundance of multiply-substituted isotopologues are of geochemical interest because of their potential for use as an isotopic geothermometer that can be accessed via analyses of a single compound (Wang et al., 2004; Eiler, 2007). Furthermore, clumped isotopologue data provide another dimension for probing kinetic and equilibrium isotope effects and for constraining isotope exchange processes in natural settings (e.g., Eiler and Schauble, 2004; Yeung et al., 2012, and Yeung, 2016). For example, the isotope exchange reaction



84 has an equilibrium constant  $K$  that varies between  $\sim 1.007$  at  $0^\circ\text{C}$  to  $1.000$  at temperatures approaching infinity (at  
85 which isotopes are randomly distributed amongst all possible isotopologues, i.e., the stochastic distribution) (see  
86 Wang et al., 2015, and references therein for details regarding calculations from which  $K$  is obtained).

87 Subsequent surveys of methane in the environment revealed that in methane of microbial origin produced in both  
88 natural settings and pure cultures, the reaction quotient ( $Q$ , see also Sec. 2.2) of Reaction 2 varies between  $0.997$   
89 and  $1.007$  (Stolper et al., 2014a; Inagaki et al., 2015; Stolper et al., 2015; Wang et al., 2015; Douglas et al., 2016),  
90 a range that is much larger than that expected for thermodynamic equilibrium (ca.  $1.004$  to  $1.007$ ) at temperatures  
91 at which microbial life is possible ( $\sim 0$  to  $120^\circ\text{C}$ ; Takai et al., 2008) (Wang et al., 2015). The nonequilibrium  
92 isotope signatures were attributed to intrinsic clumped isotopologue effects expressed during biological  
93 methanogenesis under conditions of low reversibility (Stolper et al., 2015; Wang et al., 2015). Using inferences  
94 based on  $\delta^{13}\text{C}$  and  $\delta\text{D}$  data, methane oxidation was excluded as a significant origin of the nonequilibrium isotope  
95 signals (Wang et al., 2015). However, experimental constraints on the fractionation of  $^{13}\text{CH}_3\text{D}$  during biological  
96 methane oxidation are lacking in the clumped isotope literature.

97 In this paper, we report experimental measurements of the fractionation of  $^{13}\text{CH}_3\text{D}$  during aerobic methane  
98 oxidation by cultures of the bacterium *Methylococcus capsulatus* (Bath). It is demonstrated that aerobic  
99 methanotrophy affects the abundance of  $^{13}\text{CH}_3\text{D}$  in a predictable fashion relative to  $\delta^{13}\text{C}$  and  $\delta\text{D}$ ; the directionality  
100 and magnitude of these effects depend on whether oxidation occurs in a closed or open system. We present  
101 simple models to illustrate the expected shifts in  $^{13}\text{CH}_3\text{D}$  abundance under different scenarios, and review  
102 available environmental clumped isotopologue data in light of the new experimental constraints.

## 103 2. METHODS

### 104 2.1. Cultures

105 *Methylococcus capsulatus* strain Bath cultures were grown in 10 ml of nitrate mineral salts medium supplemented  
106 with  $5\ \mu\text{M}$   $\text{CuSO}_4$  (Welander and Summons, 2012). Serum bottles ( $160\ \text{cm}^3$ ) were inoculated with 2% (v/v)  
107 inoculum from a starter culture that had grown for ca. 30 hours, stoppered and sealed without removing ambient  
108 air, and injected with  $20\ \text{cm}^3$  SATP ( $\sim 810\ \mu\text{mol}$ ) of methane from commercially-sourced cylinders using a gas-  
109 tight syringe. Tests indicated that the starting gas compositions were consistent within analytical error ( $\pm 5\%$ )  
110 between serum bottles. Multiple serum bottles were inoculated for each of the two experimental temperatures  
111 (Table 1). Cultures were incubated at  $30$  or  $37^\circ\text{C}$  while shaking at  $225\ \text{rpm}$  and sacrificed at given times by  
112 adding  $1\ \text{ml}$  of  $1\ \text{M}$  hydrochloric acid. Each row in Table 1 shows the composition of one serum bottle at the time  
113 at which the experiment was stopped. Experimental timepoints were selected based on monitoring of growth  
114 during preliminary incubations of starter cultures (by tracking optical density, see Supplementary Fig. 1).  
115 However, to minimize puncturing of the serum bottles during the isotopic fractionation experiments, optical  
116 densities were not measured for the samples analyzed for isotopologues shown in Table 1. The combination of  
117 constant agitation, a large headspace volume relative to liquid volume, and high initial  $\text{CH}_4$  partial pressures ( $>0.1$   
118 atm) ensures that diffusion into the liquid from the headspace does not limit the rate of methane consumption  
119 (Templeton et al., 2006; Nihous, 2008).

## 120 2.2. Analytical techniques

121 Concentrations of headspace gases, including CH<sub>4</sub> and CO<sub>2</sub>, were determined via gas chromatography (GC) using  
122 a Shimadzu GC-2014 gas chromatograph configured with a packed column (Carboxen-1000, 5' × 1/8", Supelco,  
123 Bellefonte, Pennsylvania, USA) held at 140 °C and argon carrier gas, and thermal conductivity and methanizer-  
124 flame ionization detectors. Subsamples of the headspace (0.20 cm<sup>3</sup> at laboratory temperature, ~23 °C) from each  
125 serum bottle were taken via a gas-tight syringe and injected onto the column. Gas concentrations were  
126 determined directly as partial pressures. Accuracy of the analyses, evaluated from standards, was ±5%. The  
127 fraction of initial methane remaining, *f*, in each batch culture was calculated from these measurements (Table 1),  
128 with uncertainties propagated following Ku (1969).

129 Samples of methane were purified via cryofocusing–preparative gas chromatography through a packed column  
130 (Carboxen-1000, 5' × 1/8", Supelco) held at 30 °C with helium carrier gas, and cryotrapping of the eluted methane  
131 on activated charcoal at liquid nitrogen temperature (Wang et al., 2015). The relative abundances of the methane  
132 stable isotopologues <sup>12</sup>CH<sub>4</sub>, <sup>13</sup>CH<sub>4</sub>, <sup>12</sup>CH<sub>3</sub>D, and <sup>13</sup>CH<sub>3</sub>D were measured using a tunable infrared laser direct  
133 absorption spectroscopy technique described previously (Ono et al., 2014; Wang et al., 2015).

134 Isotope values are reported herein using standard delta-notation.<sup>1</sup> In accordance with IUPAC recommendations  
135 (Coplen, 2011), we have omitted the factor of 1000‰ from the definition of δ and other isotope values (including  
136 Δ<sup>13</sup>CH<sub>3</sub>D, below). Carbon and hydrogen isotope values were calibrated against community reference materials  
137 NGS-1 and NGS-3 (Wang et al., 2015).

138 The abundance of <sup>13</sup>CH<sub>3</sub>D is tracked via the Δ<sup>13</sup>CH<sub>3</sub>D value, defined according to Ono et al. (2014) as:

$$139 \quad \Delta^{13}\text{CH}_3\text{D} = \ln Q, \text{ where } Q = \frac{[^{13}\text{CH}_3\text{D}][^{12}\text{CH}_4]}{[^{13}\text{CH}_4][^{12}\text{CH}_3\text{D}]} \quad (3)$$

140 Here, *Q* is the reaction quotient for Reaction 2, and Δ<sup>13</sup>CH<sub>3</sub>D ≈ *Q* – 1 because *Q* is close to unity in the natural  
141 and experimental systems studied herein.<sup>2</sup> For a methane sample that has attained a distribution of isotopes  
142 among all isotopologues consistent with equilibrium at a given temperature, *Q* = *K*. The temperature dependence  
143 of the equilibrium Δ<sup>13</sup>CH<sub>3</sub>D value was theoretically estimated and experimentally calibrated previously (Wang et  
144 al., 2015).

145 Methane samples with a wide range of δD values (ca. –480‰ to +500‰ vs. SMOW) were prepared and  
146 thermally-equilibrated over platinum catalyst at 300 °C to correct for the nonlinearity in the spectroscopic analysis  
147 described by Ono et al. (2014).

## 148 2.3. Calculation of isotope and isotopologue fractionation factors

149 The MMO-catalyzed reaction between methane and O<sub>2</sub> to produce the intermediate product methanol is the first  
150 in a sequence of enzymatic reactions involved in aerobic methanotrophy (Sirajuddin and Rosenzweig, 2015). We  
151 focus on this reaction because it is the most important isotopically-fractionating step in this sequence as it is  
152 considered to be both rate-limiting and isotope-sensitive (Nesheim and Lipscomb, 1996) under the studied  
153 experimental conditions. Limitation of the rate of methane consumption by this step requires that methane

<sup>1</sup>Definitions: δ<sup>13</sup>C = (<sup>13</sup>C/<sup>12</sup>C)<sub>sample</sub>/(<sup>13</sup>C/<sup>12</sup>C)<sub>PDB</sub> – 1, and δD = (D/H)<sub>sample</sub>/(D/H)<sub>SMOW</sub> – 1 [for natural samples of methane, δ<sup>13</sup>C ≈ (<sup>13</sup>CH<sub>4</sub>/<sup>12</sup>CH<sub>4</sub>)<sub>sample</sub>/(<sup>13</sup>CH<sub>4</sub>/<sup>12</sup>CH<sub>4</sub>)<sub>PDB</sub> – 1 and δD ≈ 1/4 (<sup>12</sup>CH<sub>3</sub>D/<sup>12</sup>CH<sub>4</sub>)<sub>sample</sub>/(D/H)<sub>SMOW</sub> – 1].

<sup>2</sup> From the approximation ln(1 + *x*) ≈ *x* for values of *x* close to zero.

154 diffusion into and out of the cells be rapid relative to MMO catalysis. Following Nihous (2010), we assume that  
 155 isotopic fractionation associated with transfer of methane across cell membranes is negligible.

156 The reaction scheme for the first step of the aerobic oxidation of the methane isotopologues  $^{12}\text{CH}_4$ ,  $^{13}\text{CH}_4$ ,  
 157  $^{12}\text{CH}_3\text{D}$ , and  $^{13}\text{CH}_3\text{D}$  can be described by the following six chemical reactions:



164 *2.3.1. Carbon isotope fractionation*

165 Assuming that the reaction is irreversible, follows first-order kinetics, and occurs in a closed system, the  
 166 following differential equations can be written for  $^{12}\text{CH}_4$  and  $^{13}\text{CH}_4$ :

167 
$$\frac{d^{12}\text{CH}_4}{dt} = -k \cdot [^{12}\text{CH}_4] \quad (10)$$

168 
$$\frac{d^{13}\text{CH}_4}{dt} = -^{13}\alpha \cdot k \cdot [^{13}\text{CH}_4] \quad (11)$$

169 where  $k$  is the rate constant for  $^{12}\text{CH}_4$  consumption (Reaction 4), and  $^{13}\alpha$  is the fractionation factor for  $^{13}\text{C}/^{12}\text{C}$   
 170 (ratio of rate constants for Reactions 5 and 4).

171 Combining Eqns. 10 and 11, eliminating  $dt$ , and integrating from  $f = 1$  (initial) to  $f$  yields the equation:

172 
$$\ln\left(\frac{[^{13}\text{CH}_4]_f}{[^{13}\text{CH}_4]_{\text{init}}}\right) = ^{13}\alpha \cdot \ln\left(\frac{[^{12}\text{CH}_4]_f}{[^{12}\text{CH}_4]_{\text{init}}}\right) \quad (12)$$

173 Subtracting  $\ln\left(\frac{[^{12}\text{CH}_4]_f}{[^{12}\text{CH}_4]_{\text{init}}}\right)$  from each side, and using the approximations  $f \approx \frac{[^{12}\text{CH}_4]_f}{[^{12}\text{CH}_4]_{\text{init}}}$   
 174 and  $\frac{[^{13}\text{CH}_4]_f}{[^{12}\text{CH}_4]_f} \approx \frac{[^{13}\text{C}]}{[^{12}\text{C}]}$ , a form of the classic ‘‘Rayleigh equation’’ is obtained (Mariotti et al., 1981):

175 
$$\ln\frac{\delta^{13}\text{C}+1}{\delta^{13}\text{C}_{\text{init}}+1} = (^{13}\alpha - 1) \ln f \quad (13)$$

176 *2.3.2. Hydrogen isotope fractionation*

177 For the D-substituted isotopologue  $^{12}\text{CH}_3\text{D}$ , there are two ways to break a carbon-hydrogen bond. These two  
 178 pathways are described by Reactions 6 and 7. The former involves the breakage of the C–D bond (accompanied  
 179 by a primary isotope effect, described by the fractionation factor  $^{\text{D}}\alpha_{\text{p}}$ ), while the latter involves the breakage of  
 180 any of the three C–H bonds *adjacent* to the C–D bond (incurring a secondary isotope effect,  $^{\text{D}}\alpha_{\text{s}}$ ). Thus, the  
 181 overall rate of the oxidation of  $^{12}\text{CH}_3\text{D}$  to methanol can be described by:

182 
$$\frac{d^{12}\text{CH}_3\text{D}}{dt} = -\frac{1}{4} \cdot {}^D\alpha_p \cdot k \cdot [^{12}\text{CH}_3\text{D}] - \frac{3}{4} \cdot {}^D\alpha_s \cdot k \cdot [^{12}\text{CH}_3\text{D}] \quad (14)$$

183 By lumping together  ${}^D\alpha_p$  and  ${}^D\alpha_s$ , the rate equation can be simplified to:

184 
$$\frac{d^{12}\text{CH}_3\text{D}}{dt} = -{}^D\alpha \cdot k \cdot [^{12}\text{CH}_3\text{D}], \quad (15)$$

185 where  ${}^D\alpha = \frac{1}{4} {}^D\alpha_p + \frac{3}{4} {}^D\alpha_s$ .

186 This parameterization of D/H fractionation is attractive in that it allows for apparent overall isotopic fractionation  
 187 factors to be constrained by cell culture experiments and measurement with conventional geochemical techniques  
 188 (e.g., isotope ratio mass spectrometry), without measurement of the individual reaction products. Applying the  
 189 same logic used in Sec. 2.3.1, the following expression is obtained:

190 
$$\ln \frac{\delta^{D+1}}{\delta^{D_{\text{init}}+1}} = ({}^D\alpha - 1) \ln f \quad (16)$$

191 Combining Eqns. 13 and 16 yields an equation describing the correlation between carbon and hydrogen isotope  
 192 fractionation:

193 
$$\ln \frac{\delta^{D+1}}{\delta^{D_{\text{init}}+1}} = \left( \frac{{}^D\alpha - 1}{{}^{13}\alpha - 1} \right) \ln \frac{\delta^{13}\text{C}+1}{\delta^{13}\text{C}_{\text{init}}+1} \quad (17)$$

### 194 2.3.3. $^{13}\text{CH}_3\text{D}$ fractionation

195 The rate of oxidation of  $^{13}\text{CH}_3\text{D}$  can be described by:

196 
$$\frac{d^{13}\text{CH}_3\text{D}}{dt} = -\frac{1}{4} \cdot \gamma_p \cdot {}^{13}\alpha \cdot {}^D\alpha_p \cdot k \cdot [^{13}\text{CH}_3\text{D}] - \frac{3}{4} \cdot \gamma_s \cdot {}^{13}\alpha \cdot {}^D\alpha_s \cdot k \cdot [^{13}\text{CH}_3\text{D}] \quad (18)$$

197 Here, we have introduced the terms  $\gamma_p$  and  $\gamma_s$  to characterize deviations of the clumped isotopologue fractionation  
 198 factor from the product of the  $^{13}\text{C}/^{12}\text{C}$  and D/H fractionation factors ( $\alpha$  values). When there is no deviation from  
 199 this product (i.e., primary and secondary isotope fractionation factors for bond breakage in  $^{13}\text{CH}_3\text{D}$  follow what is  
 200 referred to hereafter as the “product rule”), both  $\gamma_p$  and  $\gamma_s$  are unity. Deviations from the product rule represent a  
 201 “clumped isotopologue effect” on bond breakage that arises from the substitution of both  $^{13}\text{C}$  and D in the  
 202 substrate methane. To simplify the treatment of clumped isotopologue effects in the absence of literature data for  
 203  $\gamma_p$  and  $\gamma_s$ , we adopt the following form of the rate equation:

204 
$$\frac{d^{13}\text{CH}_3\text{D}}{dt} = -\gamma \cdot {}^{13}\alpha \cdot {}^D\alpha \cdot k \cdot [^{13}\text{CH}_3\text{D}] \quad (19)$$

205 Here, the “gamma-factor” ( $\gamma$ ) is an empirically-constrained term that describes an *effective* clumped isotopologue  
 206 fractionation factor. Implicit in the use of Eqn. 19 is that  $\gamma \cdot {}^D\alpha = \frac{1}{4} \cdot \gamma_p \cdot {}^D\alpha_p + \frac{3}{4} \cdot \gamma_s \cdot {}^D\alpha_s$  (from the definition  
 207 of  ${}^D\alpha$  in Sec. 2.3.2; also see discussion in Sec. 4.1.2). This condition is satisfied, although not uniquely, when  $\gamma$  is  
 208 equal to both  $\gamma_p$  and  $\gamma_s$ .

209 Equation 19 is convenient because it allows for  $\gamma$  to be constrained by measurements of the methane  
 210 isotopologues in experiments conducted at natural abundance without the use of isotopically labeled substrates or  
 211 measurement of individual isotopically-substituted products. Integration of Eqn. 19 combined with Eqn. 10,

212 subtraction of the isotopologue-ratio forms of Eqns. 13 and 16 from the result, and substitution of the definition of  
213  $\Delta^{13}\text{CH}_3\text{D}$  (Eqn. 3) yields:

$$214 \quad \Delta^{13}\text{CH}_3\text{D} = \Delta^{13}\text{CH}_3\text{D}_{\text{initial}} + (\gamma \cdot {}^{13}\alpha \cdot {}^{\text{D}}\alpha - {}^{13}\alpha - {}^{\text{D}}\alpha + 1) \cdot \ln f \quad (20)$$

215 By adopting this greatly simplified treatment, it necessarily means that differences in primary and secondary  
216 isotope effects for different forms of the enzyme in different methanotroph species are masked and lumped into an  
217 “effective” fractionation factor. A similar line of reasoning was used by Stolper et al. (2015) to simplify the  
218 representation of a model methanogenic system.

### 219 3. RESULTS

220 During the course of the experiments at 30 and 37 °C, the concentration of methane in the headspace decreased  
221 and the concentration of CO<sub>2</sub> increased (Table 1). The bottles incubated at 37 °C exhibited a lag phase (observed  
222 in preliminary experiments with starter cultures, Supplementary Fig. 1), with a rapid transition into active  
223 methane consumption around 41 hours after inoculation (Table 1), whereas in the 30 °C experiments, methane  
224 consumption began immediately after inoculation, but at an apparently lower rate. Based on mass balance of  
225 measured CO<sub>2</sub> and CH<sub>4</sub> concentrations relative to initial CH<sub>4</sub> (Table 1), ~7% to 41% of carbon was not accounted  
226 for; this fraction of carbon was likely incorporated into cellular biomass (*b* in Eqn. 1). This range of *b* values is  
227 similar to ranges observed in previous studies (e.g., 0.1–0.5 in Templeton et al., 2006).

228 The initial isotopic composition of the methane used was different between the two sets of experiments (Table 1).  
229 As methane was consumed, the  $\delta^{13}\text{C}$  and  $\delta\text{D}$  values of the residual methane increased (Fig. 1), indicating a  
230 preferential consumption of the lighter <sup>12</sup>C and <sup>1</sup>H by the bacteria. Conversely,  $\Delta^{13}\text{CH}_3\text{D}$  values of the residual  
231 methane decreased as methane was consumed, starting from initial values of ca. +2.6‰ and +2.2‰, and  
232 decreasing to “anticlumped” (<0‰) values of ca. -1.5‰ and -1.9‰, respectively, at the last time points sampled  
233 in the 30 and 37 °C experiments (Table 1).

234 Using Eqns. 13, 16, and 20, values of the fractionation factors <sup>13</sup> $\alpha$ , <sup>D</sup> $\alpha$ , and  $\gamma$  were calculated for each time point  
235 after the initial (Table 1). All calculations used the initial timepoint as the reference starting point; thus, the  
236 fractionation factors reported are averaged over the entire reaction occurring in the bottle, and contain correlated  
237 errors linked to the uncertainty in data from the initial timepoint. Fractionation factors were calculated for each  
238 timepoint, rather than over all bottles in an experiment, to avoid artifacts from variable growth between bottles,  
239 particularly at the lower temperature of 30 °C (see Supplementary Fig. 1). In the earlier time points, the error in  
240 the calculated fractionation factors is large because of uncertainties in *f* and in  $\Delta^{13}\text{CH}_3\text{D}$ . For each set of  
241 experiments, the weighted-averages of the fractionation factors were determined, and are listed in Table 1, and the  
242 corresponding trajectories (using experimental <sup>13</sup> $\alpha$  and <sup>D</sup> $\alpha$  values, and variable  $\gamma$ ) are depicted in Fig. 1.

243 Isotopic fractionation of D/H was substantially greater in magnitude than that of <sup>13</sup>C/<sup>12</sup>C (Fig. 2a). In general, a  
244 greater degree of both carbon- and hydrogen-isotope fractionation was observed in the bottles incubated at 37 °C  
245 than at 30 °C (Fig. 2b). No systematic changes in the magnitude of isotope fractionation were observed over the  
246 course of the experiments (Table 1). A similar, tight correlation of D/H and <sup>13</sup>C/<sup>12</sup>C fractionation is observed  
247 between the two sets of experiments (Fig. 2a).

248 Calculated  $\gamma$  values for each experimental timepoint are shown in Table 1. All values were close to unity, and  
249 showed no systematic changes over the course of incubation. The weighted-average  $\gamma$  values for the experiments

250 were identical to unity within  $2\sigma$  error ( $1.0005 \pm 0.0006$  and  $1.0000 \pm 0.0014$  for the 30 and 37 °C experiments,  
251 respectively).

## 252 4. DISCUSSION

### 253 4.1. Isotope and isotopologue fractionation during aerobic methanotrophy

#### 254 4.1.1. Fractionation of methane $^{13}\text{C}/^{12}\text{C}$ and D/H ratios

255 A wide range of carbon isotope fractionation factors [ $^{13}\epsilon$  ( $= ^{13}\alpha - 1$ ) ranging from  $-38\%$  to  $-3\%$ ] have been  
256 reported in culture- and field-based studies [see Templeton et al. (2006) and references therein]. The variable  
257 nature of the magnitude of observed carbon isotope effects complicates application of measurements of individual  
258 carbon isotope ratios in diagnosing the presence and extent of methanotrophy in the environment. As such, the  
259 use of paired  $\delta^{13}\text{C}$  and  $\delta\text{D}$  data has been suggested as a possible method of removing some levels of ambiguity  
260 associated with the sole use of carbon-isotopes (Elsner et al., 2005). Although the absolute magnitudes of isotope  
261 fractionation may vary due to “masking effects” from preceding isotopically-insensitive steps such as transport  
262 across membranes or binding to an enzyme (Feisthauer et al., 2011), a correlation between the fractionation of the  
263 carbon and hydrogen isotopes can be expected because both are principally influenced by the breakage of the C–  
264 H bond. Such a correlation was first noted by Coleman et al. (1981), with later studies (Kinnaman et al., 2007;  
265 Powelson et al., 2007; Feisthauer et al., 2011) corroborating the observations in pure culture and in enrichments  
266 from other environments. The published values of  $^{\text{D}}\epsilon/^{13}\epsilon$ , corresponding to the slope of the gray lines in Fig. 2a,  
267 range from 5.9 to 14.9, with a mean of  $8.9 \pm 2.3$  [standard deviation ( $1\sigma$ ),  $n = 15$ ]. The best-fit value of  $^{\text{D}}\epsilon/^{13}\epsilon$  for  
268 the data shown in Table 1 is 9.14, a value which appears independent of the two growth temperatures tested, and  
269 which falls near the middle of the published range.

270 The consistency of the determined  $^{\text{D}}\epsilon/^{13}\epsilon$  ratios with those in the literature provides confidence that results  
271 regarding the behavior of  $\Delta^{13}\text{CH}_3\text{D}$  (discussed below) during aerobic methane oxidation by *M. capsulatus* (Bath)  
272 can be generalizable to other strains grown under other conditions. Further experiments with these strains grown  
273 under different conditions to examine clumped isotopologue fractionation will help to determine if this hypothesis  
274 is valid. In a previous study, various strains of bacteria [including *M. capsulatus*, which has two pMMOs and one  
275 sMMO (Ward et al., 2004)] grown in batch cultures under different copper (Cu) concentrations (with pMMO  
276 expressed under Cu-rich conditions and sMMO under low Cu) demonstrated consistently correlated fractionations  
277 of carbon and hydrogen isotopes, without apparent correlation to physiology or growth condition (Feisthauer et  
278 al., 2011). Values of  $^{\text{D}}\epsilon/^{13}\epsilon$  derived from that study range from 7.3 to 8.8, and are close to the average  $^{\text{D}}\epsilon/^{13}\epsilon$  ratio  
279 from our dataset (9.14, Fig. 2a). In particular, *M. capsulatus* grown at 45 °C induced isotopic fractionations of  $^{13}\alpha$   
280  $= 0.972 \pm 0.002$  and  $^{\text{D}}\alpha = 0.769 \pm 0.030$  (published uncertainties were listed as 95% confidence interval,  
281 approximately  $2\sigma$ ) under Cu-rich conditions, and under Cu-poor conditions, similar values of  $^{13}\alpha = 0.977 \pm 0.003$   
282 and  $^{\text{D}}\alpha = 0.808 \pm 0.029$  (Feisthauer et al., 2011). The corresponding  $^{\text{D}}\epsilon/^{13}\epsilon$  ratios (with propagated  $\sim 2\sigma$   
283 uncertainties) indicated by their data are  $8.3 \pm 1.1$  and  $8.4 \pm 1.7$  under Cu-rich and Cu-poor conditions,  
284 respectively. These values are indistinguishable from the  $^{\text{D}}\epsilon/^{13}\epsilon$  ratio derived from regression through our  
285 experimental data ( $9.14 \pm 0.14$ ,  $2\sigma$ ; see Table 2). This correspondence of  $^{\text{D}}\epsilon/^{13}\epsilon$  ratios suggests that the proposed  
286 product rule for  $\gamma$  values (see Sec. 4.1.2) could be valid for *M. capsulatus* expressing either pMMO or sMMO,  
287 and may hold for many other methanotrophic strains cultured under various conditions.

288 Insights into the origin of D/H fractionation during methane oxidation have been obtained from studies which  
289 separately constrain the primary and secondary hydrogen isotope effects. Using molecular dynamics simulations,  
290 Pudzianowski and Loew (1983) calculated the isotope effects associated with the abstraction of H or D from CH<sub>4</sub>  
291 or CH<sub>3</sub>D by atomic oxygen, O(<sup>3</sup>P), as an analog for the methane monooxygenase reaction. Their results,  
292 expressed as fractionation factors, are  $^D\alpha_p = 0.0296$  and  $^D\alpha_s = 0.763$  (or 0.0179 and 0.759 when tunneling  
293 corrections were applied). Thus, the overall isotope fractionation,  $^D\alpha$  (see Eqn. 15), would be 0.580. This  
294 fractionation factor reflects a much larger magnitude of D/H fractionation than is observed in either our  
295 experiments ( $^D\alpha$  as low as 0.718) or those reported in other studies (plotted in Fig. 2b). Pudzianowski and Loew  
296 (1983) note, however, that the transition state of the CH<sub>4</sub>/CH<sub>3</sub>D + O(<sup>3</sup>P) reaction they modeled has only  
297 qualitative similarity to the transition state of the methane hydrogen abstraction/hydroxylation reaction performed  
298 by methane monooxygenase. Such fundamental differences between the two processes may explain the  
299 difference between their calculated fractionation and the experimental observations.

300 Multiple experimental determinations of the kinetic isotope effects for H or D abstraction have been reported  
301 [e.g., Green and Dalton (1989), Rataj et al. (1991) and Wilkins et al. (1994), and references therein]. Values for  
302 the primary isotope effect (corresponding to  $^D\alpha_p = 0.73$ ) and secondary isotope effect ( $^D\alpha_s = 0.93$ ) have been  
303 reported for methane oxidation by sMMO (Wilkins et al., 1994). The overall  $^D\alpha$  calculated from these values  
304 (0.88 via Eqn. 15) is not low enough to explain the observed D/H fractionations in culture (Fig. 2b). More  
305 recently, in experiments with a series of multiply-deuterated isotopologues of methane, Nesheim and Lipscomb  
306 (1996) determined that the isotopically-selective reaction of compound Q (the key intermediate that oxidizes CH<sub>4</sub>)  
307 of the MMO hydroxylase (MMOH<sub>Q</sub>) has very large primary and much smaller secondary kinetic isotope effects  
308 corresponding to  $^D\alpha_p = 0.01\text{--}0.02$  and  $^D\alpha_s = 0.9\text{--}1.0$ . Via Eqn. 15, the corresponding overall hydrogen isotope  
309 fractionation,  $^D\alpha$ , is then between  $\sim 0.68$  and  $\sim 0.76$ , a range which overlaps with the largest D/H fractionation  
310 observed in our experiments (0.718, Table 1). Note that such a direct quantitative comparison between isotope  
311 effects determined from pure cultures and those from *in vitro* experiments with labeled substrates may not be  
312 meaningful, as in culture experiments the fractionation induced by MMO is not necessarily the only factor  
313 determining isotopic fractionation. Regardless, the very large primary kinetic isotope effect implies that nearly all  
314 of the <sup>12</sup>CH<sub>3</sub>D reacts via the abstraction of H, with only a minor fraction reacting via the abstraction of D. This  
315 inference has potential implications for the interpretation of  $\gamma$  factors constrained by clumped isotopologue  
316 measurements (see Sec. 4.1.2).

317 Generally larger bulk carbon and hydrogen isotopic fractionations were observed in the 37 °C cultures, compared  
318 to those grown at 30 °C (Table 1). This trend is an apparent reversal of the normally-expected decrease of kinetic  
319 isotope effects with increasing temperature. Such an inverse temperature effect was previously observed by  
320 Coleman et al. (1981) on enrichment cultures grown at 11.5 and 26 °C. They excluded species differences as the  
321 source of the apparent trend, and speculated that the partial and differential expression of a combination of kinetic  
322 and equilibrium isotope effects could explain their results.

323 In our experiments, only one strain of bacterium was cultured, thus also excluding species differences as a reason  
324 for the observed inverse temperature trend. If some D/H exchange with cellular water occurs during C–H bond  
325 breakage and re-forming, the overall  $^D\epsilon$  fractionation factor should be of smaller magnitude than would otherwise  
326 be expected given the observed <sup>13</sup> $\epsilon$  value (as the carbon does not exchange). [The  $\delta D$  of water used in the cultures  
327 was not measured, but is estimated to be between  $-95\text{‰}$  and  $-32\text{‰}$  based on tap water data from Bowen et al.

328 (2007). Based on the calibration of Horibe and Craig (1995),<sup>3</sup> methane at D/H equilibrium with water at 30–37  
329 °C would be expected to have  $\delta D < -200\%$ , which is lower than the initial  $\delta D$  of methane in both sets of  
330 experiments.] The observation that the ratio  ${}^D\epsilon/{}^{13}\epsilon$  is nearly identical between the two temperatures (Fig. 2a)  
331 therefore argues against C–H bond re-equilibration as an explanation for smaller magnitudes of isotopic  
332 fractionation in the 30 °C experiments. Furthermore, our additional measurements of  $\Delta^{13}\text{CH}_3\text{D}$  indicate that  $\gamma$   
333 values are indistinguishable (within  $2\sigma$ , Table 1) between the two experiments, lending additional support to the  
334 conclusion that kinetic isotope fractionation dominates the observed isotope and isotopologue signals.

335 Given the above analysis, an alternate explanation must be sought to explain the observed apparent inverse  
336 temperature trend. According to the theory of kinetic isotope fractionation (e.g., Bigeleisen, 1949), predictions of  
337 decreasing kinetic isotope effects with increasing temperature are generally valid only for elementary reactions.  
338 The aerobic oxidation of methane by *M. capsulatus* consists of multiple enzymatic steps, and thus expression of  
339 intrinsic kinetic isotope effects may not be complete if the isotopically-sensitive methane monooxygenase  
340 reaction is not fully rate-limiting. In particular, models proposed to explain previously published experimental  
341 data point to the depletion of soluble methane concentrations below threshold levels required to maintain rates of  
342 mass transfer into the cell as a control on the degree to which kinetic isotope effects are expressed in culture  
343 (Nihous, 2008; Nihous, 2010; Vavilin et al., 2015). This behavior is analogous to that observed for  ${}^{34}\text{S}/{}^{32}\text{S}$  ratios  
344 during microbial sulfate reduction, where under low sulfate conditions, sulfur isotope fractionation is suppressed  
345 due to rate limitation by the isotopically-insensitive initial transport of sulfate into the cell (Harrison and Thode,  
346 1958; Rees, 1973). Substrate limitation has also been considered to explain trends associated with  ${}^{13}\text{C}/{}^{12}\text{C}$   
347 fractionation during methanogenesis under low intracellular  $\text{CO}_2$  levels (e.g., Valentine et al., 2004), and has been  
348 extensively studied in relation to  $\text{CO}_2$  levels during photosynthesis (e.g., Farquhar et al., 1982). Thus, the  
349 apparent inverse temperature trend in the data is possibly a result of masking of intrinsic isotope effects of MMO  
350 due to limitation from mass transport into the cell, although other explanations cannot be discounted.  
351 Experimental setups that allow rigorous accounting of carbon budgets and biomass density may allow for  
352 quantitative models of isotopologue systematics, similar to those created for  $\delta^{13}\text{C}$  (Templeton et al., 2006; Nihous,  
353 2008; Nihous, 2010), to be used in evaluating the potential effects of diffusion of methane to and through cells.  
354 Our data thus also encourages consideration of mass transport and bioavailable methane levels when evaluating  
355 methane isotope data in field settings where oxidation may be occurring. Despite the particular mechanisms  
356 underlying apparent inverse temperature trends remaining unclear, the general observation that the fractionation  
357 of  ${}^{13}\text{C}/{}^{12}\text{C}$  and D/H ratios observed in our study is consistent with previously reported experiments is key, as it  
358 suggests that the discussion below regarding patterns of fractionation of  ${}^{13}\text{CH}_3\text{D}$  may be generally applicable to  
359 experimental cultures of aerobic methanotrophic bacteria.

#### 360 4.1.2. Fractionation of ${}^{13}\text{CH}_3\text{D}$

361 In our batch culture experiments, the  $\Delta^{13}\text{CH}_3\text{D}$  value of residual methane decreased with progressive oxidation  
362 (Table 1). The weighted average  $\gamma$  values determined for the both the 30 °C experiment ( $1.0005 \pm 0.0006$ ,  $2\sigma$ )  
363 and the 37 °C experiment ( $1.0000 \pm 0.0014$ ) are indistinguishable from unity. Thus, the results of this study  
364 indicate that the overall kinetic fractionation factor for  ${}^{13}\text{CH}_3\text{D}/{}^{12}\text{CH}_4$  can be closely approximated as the product  
365 of the carbon and hydrogen isotopic fractionation factors (i.e.,  ${}^{13-\text{D}}\alpha \approx {}^{13}\alpha \cdot {}^D\alpha$ ). This product rule can be used to

---

<sup>3</sup> Comparisons of the fractionation factor for D/H equilibrium between  $\text{CH}_4(\text{g})$  and  $\text{H}_2\text{O}(\text{l})$  derived from the calibrations of different studies reveal a substantial range in estimates (up to 30‰ at 30–37 °C, see Wang et al., 2015). This is mainly due to uncertainty in extrapolations of experimental calibrations of  $\text{H}_2(\text{g})/\text{H}_2\text{O}(\text{g})$  at  $>200$  °C to lower temperatures. However, this level of uncertainty does not impact the interpretation developed here.

366 model the  $\Delta^{13}\text{CH}_3\text{D}$  value resulting from aerobic methane oxidation. If a higher level of prediction is necessary,  
367 precise constraints on primary and secondary  $\alpha$  and  $\gamma$  values are required (see Sec. 2.3.3 and discussion below).

368 Given low enough  $\gamma$  values (depending on  $^{13}\alpha$  and  $^{\text{D}}\alpha$ ), the  $\Delta^{13}\text{CH}_3\text{D}$  value may actually *increase* over the course  
369 of the reaction in a closed system such as a batch culture. The break-even condition, under which  $\Delta^{13}\text{CH}_3\text{D}$  does  
370 not change over the course of a closed system process, occurs when  $\gamma = (^{13}\alpha + ^{\text{D}}\alpha - 1)/(^{13}\alpha \cdot ^{\text{D}}\alpha)$ . For the 30  
371 and 37 °C experiments, the break-even  $\gamma$  values are 0.9986 and 0.9943, respectively. These values are  
372 substantially less than those determined experimentally above (the latter by a considerable  $-0.0057$  or  $-5.7\%$ ).  
373 Therefore, it should not be assumed that  $\Delta^{13}\text{CH}_3\text{D}$  values are unaffected by closed system methane oxidation.  
374 Otherwise, the apparent  $\Delta^{13}\text{CH}_3\text{D}$  temperature may be substantially overestimated or become imaginary, as shown  
375 in Fig. 3a.

376 There is no *a priori* reason that  $\gamma$  must be close to unity.<sup>4</sup> The  $\gamma$  factor as defined in Sec. 2.3.3 is empirically  
377 useful in that it is a single number that expresses the reactivity of  $^{13}\text{CH}_3\text{D}$  relative to the other isotopologues.  
378 Because  $^{13}\text{CH}_3\text{D}$  can react by two nonidentical hydrogen-abstraction reactions (Reactions 8 and 9), the  $\gamma$  value  
379 expresses the summation of the products of the hydrogen-isotope effects ( $^{\text{D}}\alpha_{\text{p}}$  and  $^{\text{D}}\alpha_{\text{s}}$ ) and the “clumped  
380 isotopologue effects” ( $\gamma_{\text{p}}$  and  $\gamma_{\text{s}}$ ) for D in both primary and secondary sites:  $\gamma \cdot ^{\text{D}}\alpha = \frac{1}{4} \cdot \gamma_{\text{p}} \cdot ^{\text{D}}\alpha_{\text{p}} + \frac{3}{4} \cdot \gamma_{\text{s}} \cdot ^{\text{D}}\alpha_{\text{s}}$ . A  
381 conceptual exercise helpfully illustrates the relative weighting of D- vs. H-abstraction reactions expressed in the  $\gamma$   
382 factor. Assuming  $^{\text{D}}\alpha_{\text{p}} = 0.02$  and  $^{\text{D}}\alpha_{\text{s}} = 0.9$  (from Sec. 4.1.1), and  $\gamma = 0.9990$  (i.e.,  $-1\%$  from unity, which is at the  
383 lower edge of  $2\sigma$  uncertainty on the weighted average  $\gamma$  values for the experiments shown in Table 1), then  $^{\text{D}}\alpha =$   
384  $0.68$  and  $0.6786 = 0.0050 \cdot \gamma_{\text{p}} + 0.6750 \cdot \gamma_{\text{s}}$ . Assigning a value to either  $\gamma_{\text{p}}$  or  $\gamma_{\text{s}}$  would constrain the other;  
385 hence, two extreme cases can be considered: (i) if  $\gamma_{\text{s}} = 1$ , then  $\gamma_{\text{p}} = 0.86$ ; or alternatively (ii) if  $\gamma_{\text{p}} = 1$ , then  $\gamma_{\text{s}} =$   
386  $0.9990$ . The former case requires a large primary clumped isotopologue effect because proportionally very few  
387  $^{13}\text{CH}_3\text{D}$  (and  $^{12}\text{CH}_3\text{D}$ ) molecules react through direct D-abstraction rather than H-abstraction (see Sec. 4.1.1),  
388 whereas the latter requires only a much smaller secondary clumped isotopologue effect on H-abstraction from  
389  $^{13}\text{CH}_3\text{D}$  to explain a  $\gamma$  value that deviates slightly from unity. Although insufficient constraints on either  $\gamma_{\text{p}}$  or  $\gamma_{\text{s}}$   
390 are currently available, this exercise indicates that a small secondary clumped isotopologue effect (i.e.,  $\gamma_{\text{s}} \neq 1$  but  
391 is very close) could exist, but may be hardly detectable. Given the uncertainties surrounding experimental  
392 determinations of  $^{\text{D}}\alpha_{\text{p}}$  and  $^{\text{D}}\alpha_{\text{s}}$  (discussed in Sec. 4.1.1), accurate values of  $\gamma_{\text{p}}$  and  $\gamma_{\text{s}}$  cannot yet be assigned. For  
393 geochemical applications, the  $\gamma$  factor is at present best used as an empirically-fitted parameter, similar to the  
394 manner in which the overall D/H fractionation factor  $^{\text{D}}\alpha$  is typically treated.

395 Irrespective of the exact magnitude of the  $\gamma$  factor, it is clear that  $\Delta^{13}\text{CH}_3\text{D}$  becomes less clumped with  
396 progressive oxidation in a closed system under the growth conditions tested in this study. Because of the  
397 consistency of our  $^{\text{D}}\epsilon/^{13}\epsilon$  results with previous experiments with organisms also using pMMO and/or sMMO (Fig.  
398 2a), it is not unreasonable to expect similar results on  $\Delta^{13}\text{CH}_3\text{D}$  values for methane oxidation by other strains of  
399 aerobic methanotrophic bacteria.

400 As mentioned above (Sec. 4.1.1), a possible explanation for the differences in the hydrogen isotopic fractionation  
401 factor for the experiments at the two temperatures relates to partial expression of equilibrium isotope effects in

---

<sup>4</sup> For example, when methane effuses through a small orifice,  $\gamma$  (when defined as the ratio of the isotopologue fractionation factor for  $^{13}\text{CH}_3\text{D}/^{12}\text{CH}_4$  to the product of those for  $^{13}\text{CH}_4/^{12}\text{CH}_4$  and  $^{12}\text{CH}_3\text{D}/^{12}\text{CH}_4$ ) will not be unity. From the kinetic theory of gases, the rate of effusion of an isotopologue is proportional to  $(\text{mass})^{-1/2}$ , such that  $\gamma = 1.00174$ . Escaping methane will have lower (lighter)  $\delta^{13}\text{C}$  and  $\delta\text{D}$ , but *higher*  $\Delta^{13}\text{CH}_3\text{D}$ , than the residual methane. For a more thorough discussion, readers are referred to Eiler and Schauble (2004).

402 one or both experiments. Evidence against this explanation derives from the observation that  $\Delta^{13}\text{CH}_3\text{D}$  values of  
 403 residual methane in both experiments follow the predictions of the product rule (i.e.,  $\gamma$  values are  $\sim 1$ ); therefore it  
 404 is unlikely that there is a greater degree of C–H bond re-equilibration during the course of reaction in one  
 405 experiment over another. Thus, clumped isotopologue data also assist in diagnosing presence or absence of  
 406 isotope exchange during enzymatic abstraction of H from methane by MMO, and are consistent with a minor (not  
 407 detectable) degree of reversibility for this process. The minor degree of reversibility indicated by the data for  
 408 aerobic methane oxidation here contrasts sharply with the anaerobic oxidation of methane (AOM), an oxidation  
 409 process in which much greater degrees of reversibility have been demonstrated using carbon and hydrogen  
 410 isotopes (Holler et al., 2011; Yoshinaga et al., 2014). The environmental implications are discussed in Sec. 4.2.2.

## 411 **4.2. Implications for biogeochemical systems**

### 412 *4.2.1. Methane isotope and isotopologue fractionation in open systems*

413 In closed systems, e.g., batch cultures, no steady-state is obtained because of the lack of mass transfer to replenish  
 414 the methane consumed by methane oxidation. However, in natural systems operating close to steady-state, there  
 415 is replenishment of methane from lateral transport or diffusion, as well as methanogenesis, and there may be  
 416 multiple sinks, including methane oxidation and mass transport (Fig. 4).

417 Experimental alternatives to batch cultures, namely flow-through bioreactors (chemostats), have been used to  
 418 more directly approach the calibration of isotopic fractionation factors due to microbial metabolism in natural  
 419 settings. For example, Templeton et al. (2006) grew pure and mixed cultures of aerobic methanotrophs in  
 420 chemostats to determine the carbon isotope fractionation between methane and product methanol as a function of  
 421 environmental and physiological conditions. In such an open system, there is a constant influx of reactant  
 422 methane, which at steady-state is balanced by the sum of methane oxidation and methane carried in the effluent  
 423 out of the bioreactor (i.e., dilution).

424 In the simple limiting case where the fraction of methane removed by oxidation approaches 100% (i.e., no  
 425 methane escapes the system intact), there is effectively one sink of methane, with fractionation factors  $^{13}\alpha$ ,  $^{\text{D}}\alpha$ , and  
 426  $\gamma$  accompanying the removal process. At steady state, the isotopic values of methane in the bioreactor would be  
 427  $\delta^{13}\text{C} = (\delta^{13}\text{C}_{\text{in}} + 1) / ^{13}\alpha - 1$  and  $\delta\text{D} = (\delta\text{D}_{\text{in}} + 1) / ^{\text{D}}\alpha - 1$ , where  $\delta_{\text{in}}$  represents the isotopic composition of the  
 428 influent methane. For  $^{13}\text{CH}_3\text{D}$ , it can be shown that

$$429 \quad \Delta^{13}\text{CH}_3\text{D} = \Delta^{13}\text{CH}_3\text{D}_{\text{in}} - \ln \gamma \quad (21)$$

430 as presented in Joelsson et al. (2015). Since  $\gamma \approx 1$ , this expression can be approximated by  $\Delta^{13}\text{CH}_3\text{D} = \Delta^{13}\text{CH}_3\text{D}_{\text{in}}$   
 431  $- (\gamma - 1)$ . In our batch culture experiments at 30 and 37 °C, respectively, weighted-average values for  $(\gamma - 1)$  of  
 432  $+0.5 \pm 0.3\text{‰}$  and  $0.0 \pm 0.7\text{‰}$  ( $1\sigma$ ) were obtained (Table 1). Although steady-state experiments were not  
 433 conducted in the current study, if it is assumed that these values are also characteristic of true open-system  
 434 isotopologue fractionation factors, then the above expression can be used to place bounds on the isotopologue  
 435 composition of methane in the limiting case outlined above. Examples of the calculated methane  
 436 isotopic/isotopologue compositions are shown for model scenarios in Fig. 5a (corresponding to the endmember  
 437 labeled “fully oxidative” on each curve).

438 Equation 21 also shows that in a system at steady-state where methane is solely removed by one process (here,  
 439 oxidation), the  $\Delta^{13}\text{CH}_3\text{D}$  value is determined solely by the  $\Delta^{13}\text{CH}_3\text{D}$  value of the methane source and the  $\gamma$  factor,  
 440 in contrast to closed systems where  $\Delta^{13}\text{CH}_3\text{D}$  of residual methane is influenced also by the isotopic fractionations

441 for bulk  $^{13}\text{C}/^{12}\text{C}$  and D/H. However, in more complex systems with multiple removal processes and associated  
442 fractionation factors, the partitioning of flows among the removal processes must be considered (Hayes, 2001).

443 One example of such an open system is shown in Fig. 4. Here, methane is carried into the system via advection,  
444 and removed by both advection and oxidation. Oxidation of methane has associated fractionation factors  $^{13}\alpha$ ,  $^{\text{D}}\alpha$ ,  
445 and  $\gamma$ , whereas transport processes are assumed to cause no fractionation (Alperin et al., 1988), i.e., values of  $\alpha$   
446 and  $\gamma$  are unity. The fraction of methane removed via oxidation,  $\varphi_{\text{ox}}$ , describes the partitioning of flows among  
447 the two methane sinks. It can be shown that at steady state, the hydrogen isotopic composition of the methane in  
448 the reservoir is (Hayes, 2001):

$$449 \quad \delta\text{D} = \frac{\delta\text{D}_{\text{in}} + 1}{1 + \varphi_{\text{ox}}(^{\text{D}}\alpha - 1)} - 1 \quad (22)$$

450 An analogous equation (not shown) describes the carbon isotopic composition of methane in this system at steady  
451 state. When the  $\delta^{13}\text{C}$  and  $\delta\text{D}$  values are plotted against each other, it can be seen that the trajectory describing the  
452 continuum between the fully-advective ( $\varphi_{\text{ox}} = 0$ ) and fully-oxidative ( $\varphi_{\text{ox}} = 1$ ) endmembers is slightly curved  
453 (though approximately linear at most scales of interest, Fig. 5b).

454 For this system, unlike in the simple fully-oxidative case described by Eqn. 21, the abundance is affected not only  
455 by the  $\gamma$  value, but also by the  $^{13}\alpha$  and  $^{\text{D}}\alpha$  values:

$$456 \quad \Delta^{13}\text{CH}_3\text{D} = \Delta^{13}\text{CH}_3\text{D}_{\text{in}} - \ln \frac{1 + \varphi_{\text{ox}}(\gamma \cdot ^{13}\alpha \cdot ^{\text{D}}\alpha - 1)}{(1 + \varphi_{\text{ox}}(^{13}\alpha - 1))(1 + \varphi_{\text{ox}}(^{\text{D}}\alpha - 1))} \quad (23)$$

457 This results in a parabolic curve connecting the fully-advective and fully-oxidative endmembers (Fig. 5a). For  
458 aerobic methane oxidation, the curvature on Fig. 5a is always expected to be concave up, because both the  $^{13}\alpha$  and  
459  $^{\text{D}}\alpha$  values are less than unity. The relative position of the endmembers in  $\Delta^{13}\text{CH}_3\text{D}$  space is determined by the  $\gamma$   
460 value. When  $\varphi_{\text{ox}} = 1$ , Eqn. 23 reduces to Eqn. 21.

#### 461 4.2.2. $\Delta^{13}\text{CH}_3\text{D}$ as an environmental tracer of methane sink processes

462 Both biological and chemical processes are important sinks in the methane budget. In terrestrial ecosystems and  
463 oxygenated marine water columns, aerobic methanotrophy dominates, whereas in sulfate-rich marine sediments  
464 and gas seeps, anaerobic consumption of methane becomes important (Cicerone and Oremland, 1988; Reeburgh,  
465 2007; Valentine, 2011; Boetius and Wenzhöfer, 2013). In the atmosphere, the primary sink (~90%) is the  
466 reaction with tropospheric OH, with small contributions from microbial oxidation in soils, loss to stratosphere,  
467 and reaction with tropospheric Cl (Kirschke et al., 2013).

468 These methane-consuming processes impart distinct carbon- and hydrogen-isotopic fractionations. In general,  
469 biological processes (including aerobic methane oxidation, anaerobic oxidation of methane, and nitrite-dependent  
470 anaerobic methane oxidation) have  $^{\text{D}}\epsilon/^{13}\epsilon$  ratios between 6 and 15, whereas the atmospheric sinks,  $\text{CH}_4 + \text{OH}$  and  
471  $\text{CH}_4 + \text{Cl}$ , have  $^{\text{D}}\epsilon/^{13}\epsilon$  ratios ~58 and ~5.5, respectively (Table 2). The consistent and sizable differences in  
472 isotopic behavior among the two atmospheric processes vs. biological processes is useful for constraining the  
473 balance of different sources and sinks of methane (e.g., Kai et al., 2011; Rigby et al., 2012; Whiticar and  
474 Schaefer, 2007).

475 The behavior of methane clumped isotopologues in atmospheric reactions has also been studied. Recently,  
476 Joelsson et al. (2014) and Joelsson et al. (2015) reported the fractionation factor for  $^{13}\text{CH}_3\text{D}$  in relative-rate

477 experiments on the reactions of Cl and OH, respectively. Their experiments were conducted with mixtures of  
478  $^{12}\text{CH}_4$  and  $^{13}\text{CH}_3\text{D}$  (and also  $^{12}\text{CH}_3\text{D}$  in the OH study). Based on their measurements, the  $\gamma$  value associated with  
479 methane oxidation by Cl was  $0.980 \pm 0.019$ , and by OH was  $0.978 \pm 0.028$  ( $2\sigma$ , Table 2). The  $\gamma$  value for Cl  
480 oxidation is slightly less than unity, implying that less of the  $^{13}\text{CH}_3\text{D}$  is oxidized than would be predicted by the  
481 product rule, whereas the  $\gamma$  value for OH oxidation is within error of unity. However, the uncertainty on  
482 calculated  $\gamma$  values is large (ca. 20 to 30‰) due to limitations associated with the experimental setup and  
483 detection technique. Because  $\Delta^{13}\text{CH}_3\text{D}$  in the environment has a ca. 10‰ range (Wang et al., 2015), more precise  
484 isotopologue-specific measurements of methane in experiments conducted at natural abundance will be necessary  
485 in order to constrain clumped isotopologue fractionations in atmospheric contexts. These experiments have been  
486 conducted, and the results are reported in a companion article (Whitehill et al., **in revision**); a summary of their  
487 results are shown in Table 2.

488 In the present study,  $\gamma$  values for aerobic methane oxidation were determined ( $1.0004 \pm 0.0006$ ,  $2\sigma$ , Table 2).  
489 These values indicate that the abstraction of H from methane by methane monooxygenase is associated with little  
490 to no reversibility (see discussion in Sec. 4.1.2). This interpretation is consistent with the strong energetic  
491 favorability of methane oxidation to methanol and downstream products in the presence of abundant  $\text{O}_2$ , a strong  
492 electron acceptor (Cicerone and Oremland, 1988; Hanson and Hanson, 1996).

493 The new experimental constraints on clumped isotopologue fractionation during aerobic methane oxidation also  
494 afford an opportunity to briefly evaluate whether aerobic methane oxidation has influenced methane clumped  
495 isotopologue data available in the literature from various environments. In particular, because methane oxidation  
496 demonstrably produces nonequilibrium clumped isotopologue signatures in both closed and open systems  
497 considered in this study (Figs. 3 and 5, respectively), the out-of-equilibrium clumped isotopologue signatures in  
498 samples from Upper and Lower Mystic Lakes (Massachusetts, USA), Swamp Y (Massachusetts, USA), and The  
499 Cedars (California, USA) are considered again here (Wang et al., 2015), as well as a sample from a pond at  
500 Caltech for which a related parameter, the  $\Delta_{18}$  value, was found to be in disequilibrium (Stolper et al., 2015). At  
501 Upper Mystic Lake (a 20-m deep seasonally-stratified freshwater lake), bubble traps were deployed  $\sim 2$  m above  
502 the lake floor; the deployment of traps at such deep depths, into the oxygen-depleted hypolimnion (Peterson,  
503 2005), was designed to minimize the possibility of aerobic methane oxidation (Wang et al., 2015). At Lower  
504 Mystic Lake (a 24-m deep meromictic density-stratified lake), the monimolimnion (from which the reported  
505 sample was taken) is anoxic (Wang et al., 2015), rendering aerobic methane oxidation unlikely. For Swamp Y  
506 and the Caltech pond, the redox state of the sediments from which the methane bubbles were stirred and extracted  
507 is unknown. At The Cedars, the extremely high levels of  $\text{H}_2$  in gases exsolving from the springs maintains  $\text{O}_2$  at  
508 vanishingly low levels (near the lower bound of  $\text{H}_2\text{O}$  stability, Morrill et al., 2013). Taken together, all methane  
509 samples from these four sites exhibit narrow ranges of  $\delta^{13}\text{C}$  values between  $-59\text{‰}$  and  $-71\text{‰}$  and  $\delta\text{D}$  values  
510 between  $-265\text{‰}$  and  $-342\text{‰}$ , but carry a wide range of nonequilibrium  $\Delta^{13}\text{CH}_3\text{D}$  values (from  $-3.4\text{‰}$  to  $+3.2\text{‰}$ )  
511 that are consistent within sites but significantly different between sites (Wang et al., 2015), and exhibit  
512 isotopologue patterns that do not discernably resemble those depicted in Figs. 3 and 5. Thus, although aerobic  
513 methane oxidation cannot be fully discounted at these four sites, the experimental constraints provided in the  
514 current study do not contraindicate the assumptions made by Wang et al. (2015) and are consistent with the  
515 hypothesis that nonequilibrium  $\Delta^{13}\text{CH}_3\text{D}$  values in microbial methane in the environment and in methanogenic  
516 cultures studied to date originate primarily from intrinsic isotopologue effects during the assembly of C–H bonds  
517 during methanogenesis (Stolper et al., 2015; Wang et al., 2015).

518 Alternative biological mechanisms for methane oxidation are also important in the environment. Of particular  
519 interest is the sulfate-dependent anaerobic oxidation of methane (AOM), which is a major sink of methane in  
520 anoxic marine sediments (Reeburgh, 1976). This process operates via a very different biochemical pathway from  
521 that used by aerobic methanotrophs. While the biochemistry of AOM has not been fully characterized, it is likely  
522 that the enzymatic pathway of AOM is the reverse of methanogenesis, and involves the same or similar key  
523 enzymes (e.g., methyl-coenzyme M reductase) for addition or removal of H from single-carbon compounds  
524 (Scheller et al., 2010). Previously, it was found that as the reversibility of methanogenesis decreased (controlled  
525 in part by levels of bioavailable H<sub>2</sub>), both the δD and Δ<sup>13</sup>CH<sub>3</sub>D values of the generated methane became lower or  
526 more negative (Wang et al., 2015); similar behavior was found in Δ<sub>18</sub> (Stolper et al., 2014a; Stolper et al., 2015).  
527 From incubations of enrichment cultures of microbial consortia performing AOM, Holler et al. (2009) determined  
528 substantial kinetic isotope fractionations associated with this process (<sup>13</sup>ε = -12‰ to -36‰ and <sup>D</sup>ε = -100‰ to  
529 -230‰). The negative D/H fractionation factor results in the residual methane becoming enriched in D. Because  
530 of the demonstrated high levels of reversibility of AOM (Holler et al., 2011) and the re-equilibration of <sup>13</sup>C/<sup>12</sup>C  
531 ratios between methane and inorganic carbon at the sulfate-methane transition zone (Yoshinaga et al., 2014), it  
532 seems reasonable to speculate that AOM may produce clumped isotope signatures distinct from those of  
533 methanogenesis (Stolper et al., 2015). In particular, the expression of a combination of kinetic and equilibrium  
534 isotope effects may be observed, such that the observed Δ<sup>13</sup>CH<sub>3</sub>D value may lie between that predicted by the  
535 product rule and that predicted for thermodynamic equilibrium. If so, then measurement of Δ<sup>13</sup>CH<sub>3</sub>D may provide  
536 a way to differentiate between AOM and aerobic methanotrophy. Alternatively, if AOM also generates Δ<sup>13</sup>CH<sub>3</sub>D  
537 approximating the product rule, then the agreement of <sup>D</sup>ε/<sup>13</sup>ε between AOM (Holler et al., 2009) and aerobic  
538 methanotrophs (Table 2) suggests that potentially, microbially-mediated oxidation of methane produces only a  
539 small and predictable range of clumped isotopologue fractionations.

540 Another process, the recently-identified nitrite-dependent anaerobic methane oxidation (Ettwig et al., 2010), may  
541 also be environmentally-relevant, though its global prevalence has yet to be established. The bacterium  
542 *Candidatus Methyloirabilis oxyfera* produces molecular oxygen intracellularly from the reduction of nitrite to  
543 nitric oxide (Ettwig et al., 2010), in the absence of environmental O<sub>2</sub>; the generated oxygen is then consumed  
544 along with methane by membrane-bound pMMO through the aerobic pathway. Because of the biochemical  
545 homology of the bond-breaking enzymatic step to that of aerobic methanotrophy, it is not unreasonable to expect  
546 that nitrite-dependent anaerobic methane oxidation would produce isotopic and clumped isotopologue patterns  
547 similar to those observed in this study. Indeed, carbon and hydrogen isotope fractionation factors for this process,  
548 as determined from culture experiments (Rasigraf et al., 2012), correlate in a manner that overlaps with aerobic  
549 methane oxidation (Table 2), lending support to this hypothesis.

## 550 5. CONCLUSIONS

551 Experimental investigation of the abundance of four methane stable isotopologues (<sup>12</sup>CH<sub>4</sub>, <sup>13</sup>CH<sub>4</sub>, <sup>12</sup>CH<sub>3</sub>D, and a  
552 clumped isotopologue, <sup>13</sup>CH<sub>3</sub>D) during oxidation of methane with O<sub>2</sub> by *Methylococcus capsulatus* (Bath) grown  
553 at 30 and 37 °C indicates that Δ<sup>13</sup>CH<sub>3</sub>D values of residual methane decrease systematically over the course of  
554 reaction in batch culture. The isotopologue fractionation factor for <sup>13</sup>CH<sub>3</sub>D/<sup>12</sup>CH<sub>4</sub> is closely approximated by the  
555 product of those for <sup>13</sup>CH<sub>4</sub>/<sup>12</sup>CH<sub>4</sub> and <sup>12</sup>CH<sub>3</sub>D/<sup>12</sup>CH<sub>4</sub>. Based on the isotopologue data, no significant degree of re-  
556 equilibration of C–H bonds in methane was detected.

557 Models were developed for simple scenarios involving variable fluxes of methane removed due to advection and  
558 oxidation. In open systems operating at steady state, Δ<sup>13</sup>CH<sub>3</sub>D values depend on the ratio of methane removed via

559 different processes, as well as the isotopologue fractionation factors associated with those processes, whereas in  
560 closed systems,  $\Delta^{13}\text{CH}_3\text{D}$  values depend also on the fraction of methane remaining. Qualitative comparisons of  
561 model predictions with available environmental  $\Delta^{13}\text{CH}_3\text{D}$  data indicate that aerobic methane oxidation has only  
562 minor, if any, influence on microbial methane samples reported to date to carry nonequilibrium  $\Delta^{13}\text{CH}_3\text{D}$  values.  
563 In combination with recent experimental and theoretical work on clumped isotopologue fractionation associated  
564 with other methane sinks, the results of this study provide necessary constraints for the development of  $^{13}\text{CH}_3\text{D}$  as  
565 a tracer of the biogeochemical and atmospheric cycling of methane.

## 566 **6. ACKNOWLEDGMENTS**

567 We thank J.H-C. Wei and W.J. Olszewski for technical assistance, and D.S. Gruen, R.E. Summons, J.W.  
568 Pohlman, J.S. Seewald, and A.R. Whitehill for discussions. D.L. Valentine and two anonymous referees are  
569 thanked for helpful and constructive reviews. Grants from the National Science Foundation (NSF EAR-1250394  
570 to S.O. and EAR-1451767 to P.V.W.), and the Deep Carbon Observatory (to S.O.) supported this study. S.O.  
571 thanks the Kerr-McGee Professorship at MIT. This research was conducted with Government support under and  
572 awarded by U.S. Department of Defense, Office of Naval Research, National Defense Science and Engineering  
573 Graduate (NDSEG) Fellowship (to D.T.W.), 32 CFR 168a.

## 574 **7. SUPPLEMENTARY DATA**

575 Supplementary data associated with this manuscript can be found in the attached document.

576

577

579 **References**

580

581 Alperin M., Reeburgh W. and Whiticar M. (1988) Carbon and hydrogen isotope fractionation resulting from  
 582 anaerobic methane oxidation. *Global Biogeochemical Cycles* **2**, 279–288.

583 Bevington P. and Robinson D. K. (2002) *Data Reduction and Error Analysis for the Physical Sciences*. 3rd ed.,  
 584 McGraw-Hill Education.

585 Bigeleisen J. (1949) The relative reaction velocities of isotopic molecules. *The journal of chemical physics* **17**,  
 586 675.

587 Boetius A. and Wenzhöfer F. (2013) Seafloor oxygen consumption fuelled by methane from cold seeps. *Nature*  
 588 *Geoscience* **6**, 725–734.

589 Bousquet P., Ciais P., Miller J., Dlugokencky E., Hauglustaine D., Prigent C., Werf G. Van der, Peylin P., Brunke  
 590 E.-G., Carouge C. and others (2006) Contribution of anthropogenic and natural sources to atmospheric  
 591 methane variability. *Nature* **443**, 439–443.

592 Bowen G. J., Ehleringer J. R., Chesson L. A., Stange E. and Cerling T. E. (2007) Stable isotope ratios of tap water  
 593 in the contiguous United States. *Water Resources Research* **43**.

594 Bowman J. P. (2014) The family Methylococcaceae. In *The Prokaryotes* Springer. pp. 411–440.

595 Chanton J., Chasar L., Glaser P. and Siegel D. (2005) Carbon and hydrogen isotopic effects in microbial methane  
 596 from terrestrial environments. In *Stable Isotopes and Biosphere-Atmosphere Interactions, Physiological*  
 597 *Ecology Series* (eds. L. B. Flanagan, J. R. Ehleringer, and D. E. Pataki). Elsevier Academic Press London. pp.  
 598 85–105.

599 Cicerone R. J. and Oremland R. S. (1988) Biogeochemical aspects of atmospheric methane. *Global*  
 600 *Biogeochemical Cycles* **2**, 299–327.

601 Coleman D. D., Risatti J. B. and Schoell M. (1981) Fractionation of carbon and hydrogen isotopes by methane-  
 602 oxidizing bacteria. *Geochimica et Cosmochimica Acta* **45**, 1033–1037.

603 Coplen T. B. (2011) Guidelines and recommended terms for expression of stable-isotope-ratio and gas-ratio  
 604 measurement results. *Rapid Commun. Mass Spectrom.* **25**, 2538–2560.

605 Dlugokencky E. J., Nisbet E. G., Fisher R. and Lowry D. (2011) Global atmospheric methane: budget, changes  
 606 and dangers. *Philosophical Transactions of the Royal Society A: Mathematical, Physical and Engineering*  
 607 *Sciences* **369**, 2058–2072.

608 Douglas P., Stolper D., Smith D., Anthony K. W., Paull C., Dallimore S., Wik M., Crill P., Winterdahl M., Eiler  
 609 J. and others (2016) Diverse origins of Arctic and Subarctic methane point source emissions identified with  
 610 multiply-substituted isotopologues. *Geochimica et Cosmochimica Acta*.

611 Eiler J. M. (2007) Clumped-isotope“ geochemistry—The study of naturally-occurring, multiply-substituted  
 612 isotopologues. *Earth and Planetary Science Letters* **262**, 309–327.

613 Eiler J. M. and Schauble E. (2004) 18O 13C 16O in Earth’s atmosphere. *Geochimica et Cosmochimica Acta* **68**,  
 614 4767–4777.

- 615 Elsner M., Zwank L., Hunkeler D. and Schwarzenbach R. P. (2005) A new concept linking observable stable  
616 isotope fractionation to transformation pathways of organic pollutants. *Environmental science & technology*  
617 **39**, 6896–6916.
- 618 Ettwig K. F., Butler M. K., Le Paslier D., Pelletier E., Mangenot S., Kuypers M. M., Schreiber F., Dutilh B. E.,  
619 Zedelius J., Beer D. de and others (2010) Nitrite-driven anaerobic methane oxidation by oxygenic bacteria.  
620 *Nature* **464**, 543–548.
- 621 Farquhar G. D., O’leary M. and Berry J. (1982) On the relationship between carbon isotope discrimination and  
622 the intercellular carbon dioxide concentration in leaves. *Australian Journal of Plant Physiology* **9**, 121–137.
- 623 Feilberg K. L., Griffith D. W., Johnson M. S. and Nielsen C. J. (2005) The <sup>13</sup>C and D kinetic isotope effects in  
624 the reaction of CH<sub>4</sub> with Cl. *International journal of chemical kinetics* **37**, 110–118.
- 625 Feisthauer S., Vogt C., Modrzynski J., Szlenkier M., Krüger M., Siegert M. and Richnow H.-H. (2011) Different  
626 types of methane monooxygenases produce similar carbon and hydrogen isotope fractionation patterns during  
627 methane oxidation. *Geochimica et Cosmochimica Acta* **75**, 1173–1184.
- 628 Green J. and Dalton H. (1989) Substrate specificity of soluble methane monooxygenase. Mechanistic  
629 implications. *Journal of Biological Chemistry* **264**, 17698–17703.
- 630 Hanson R. S. and Hanson T. E. (1996) Methanotrophic bacteria. *Microbiological Reviews* **60**, 439–471.
- 631 Harrison A. and Thode H. (1958) Mechanism of the bacterial reduction of sulphate from isotope fractionation  
632 studies. *Trans. Faraday Soc.* **54**, 84–92.
- 633 Hayes J. M. (2001) Fractionation of carbon and hydrogen isotopes in biosynthetic processes. *Reviews in*  
634 *mineralogy and geochemistry* **43**, 225–277.
- 635 Holler T., Wegener G., Knittel K., Boetius A., Brunner B., Kuypers M. M. and Widdel F. (2009) Substantial  
636 <sup>13</sup>C/<sup>12</sup>C and D/H fractionation during anaerobic oxidation of methane by marine consortia enriched in vitro.  
637 *Environmental microbiology reports* **1**, 370–376.
- 638 Holler T., Wegener G., Niemann H., Deusner C., Ferdelman T. G., Boetius A., Brunner B. and Widdel F. (2011)  
639 Carbon and sulfur back flux during anaerobic microbial oxidation of methane and coupled sulfate reduction.  
640 *Proc. Natl. Acad. Sci. U. S. A.* **108**, E1484–E1490.
- 641 Horibe Y. and Craig H. (1995) D/H fractionation in the system methane-hydrogen-water. *Geochimica et*  
642 *cosmochimica acta* **59**, 5209–5217.
- 643 Hornibrook E. R., Longstaffe F. J. and Fyfe W. S. (1997) Spatial distribution of microbial methane production  
644 pathways in temperate zone wetland soils: stable carbon and hydrogen isotope evidence. *Geochimica et*  
645 *Cosmochimica Acta* **61**, 745–753.
- 646 Inagaki F., Hinrichs K.-U., Kubo Y., Bowles M., Heuer V., Hong W.-L., Hoshino T., Ijiri A., Imachi H., Ito M.  
647 and others (2015) Exploring deep microbial life in coal-bearing sediment down to 2.5 km below the ocean  
648 floor. *Science* **349**, 420–424.
- 649 IPCC (2013) *Climate change 2013: the physical science basis. Intergovernmental panel on climate change,*  
650 *working group I contribution to the IPCC fifth assessment report (AR5)*. eds. T. F. Stocker, D. Qin, G.

- 651 Plattner, M. Tignor, S. Allen, J. Boschung, A. Nauels, Y. Xia, V. Bex, and P. Midgley, New York:  
652 Cambridge University Press.
- 653 Joelsson L., Forecast R., Schmidt J., Meusinger C., Nilsson E., Ono S. and Johnson M. (2014) Relative rate study  
654 of the kinetic isotope effect in the  $^{13}\text{CH}_3\text{D} + \text{Cl}$  reaction. *Chemical Physics Letters* **605**, 152–157.
- 655 Joelsson L., Schmidt J. A., Nilsson E., Blunier T., Griffith D., Ono S. and Johnson M. S. (2015) Development of a  
656 new methane tracer: kinetic isotope effect of  $^{13}\text{CH}_3\text{D} + \text{OH}$  from 278 to 313 K. *Atmospheric Chemistry and*  
657 *Physics Discussions* **15**, 27853–27875.
- 658 Kai F. M., Tyler S. C., Randerson J. T. and Blake D. R. (2011) Reduced methane growth rate explained by  
659 decreased Northern Hemisphere microbial sources. *Nature* **476**, 194–197.
- 660 Kinnaman F. S., Valentine D. L. and Tyler S. C. (2007) Carbon and hydrogen isotope fractionation associated  
661 with the aerobic microbial oxidation of methane, ethane, propane and butane. *Geochimica et Cosmochimica*  
662 *Acta* **71**, 271–283.
- 663 Kirschke S., Bousquet P., Ciais P., Saunois M., Canadell J. G., Dlugokencky E. J., Bergamaschi P., Bergmann D.,  
664 Blake D. R., Bruhwiler L. and others (2013) Three decades of global methane sources and sinks. *Nature*  
665 *Geoscience* **6**, 813–823.
- 666 Ku H. (1969) Notes on the use of propagation of error formulas. *J. Res. Nat. Bur. Stand. C* **70C**, 263–273.
- 667 Lau M. C., Stackhouse B., Layton A., Chauhan A., Vishnivetskaya T., Chourey K., Ronholm J., Mykytczuk N.,  
668 Bennett P., Lamarche-Gagnon G., Burton N., Pollard W., Omelon C., Medvigy D., Hettich R., Pfiﬀner S.,  
669 Whyte L. and Onstott T. (2015) An active atmospheric methane sink in high Arctic mineral cryosols. *The*  
670 *ISME journal* **9**, 1880–1891.
- 671 Mariotti A., Germon J., Hubert P., Kaiser P., Letolle R., Tardieux A. and Tardieux P. (1981) Experimental  
672 determination of nitrogen kinetic isotope fractionation: some principles; illustration for the denitrification and  
673 nitrification processes. *Plant and soil* **62**, 413–430.
- 674 Morrill P. L., Kuenen J. G., Johnson O. J., Suzuki S., Rietze A., Sessions A. L., Fogel M. L. and Nealson K. H.  
675 (2013) Geochemistry and geobiology of a present-day serpentinization site in California: The Cedars.  
676 *Geochimica et Cosmochimica Acta* **109**, 222–240.
- 677 Nesheim J. C. and Lipscomb J. D. (1996) Large kinetic isotope effects in methane oxidation catalyzed by methane  
678 monooxygenase: evidence for CH bond cleavage in a reaction cycle intermediate. *Biochemistry* **35**, 10240–  
679 10247.
- 680 Nihous G. C. (2008) A quantitative interpretation of recent experimental results on stable carbon isotope  
681 fractionation by aerobic  $\text{CH}_4$ -oxidizing bacteria. *Geochimica et Cosmochimica Acta* **72**, 4469–4475.
- 682 Nihous G. C. (2010) Notes on the temperature dependence of carbon isotope fractionation by aerobic  $\text{CH}_4$ -  
683 oxidising bacteria. *Isotopes in Environmental and Health Studies* **46**, 133–140.
- 684 Ono S., Wang D. T., Gruen D. S., Sherwood Lollar B., Zahniser M., McManus B. J. and Nelson D. D. (2014)  
685 Measurement of a Doubly-Substituted Methane Isotopologue,  $^{13}\text{CH}_3\text{D}$ , by Tunable Infrared Laser Direct  
686 Absorption Spectroscopy. *Analytical Chemistry* **86**, 6487–6494.

- 687 Oremland R. S. and Culbertson C. W. (1992) Importance of methane-oxidizing bacteria in the methane budget as  
688 revealed by the use of a specific inhibitor. *Nature* **356**, 421–423.
- 689 Peterson E. J. R. (2005) Carbon and electron flow via methanogenesis,  $\text{SO}_4^{2-}$ ,  $\text{NO}_3^-$  and  $\text{Fe}^{3+}$  reduction in  
690 the anoxic hypolimnia of upper Mystic Lake. Thesis, Massachusetts Institute of Technology.
- 691 Powelson D., Chanton J. and Abichou T. (2007) Methane oxidation in biofilters measured by mass-balance and  
692 stable isotope methods. *Environmental Science & Technology* **41**, 620–625.
- 693 Pudzianowski A. T. and Loew G. H. (1983) Hydrogen abstractions from methyl groups by atomic oxygen.  
694 Kinetic isotope effects calculated from MNDO/UHF results and an assessment of their applicability to  
695 monooxygenase-dependent hydroxylations. *The Journal of Physical Chemistry* **87**, 1081–1085.
- 696 Rasigraf O., Vogt C., Richnow H.-H., Jetten M. S. and Ettwig K. F. (2012) Carbon and hydrogen isotope  
697 fractionation during nitrite-dependent anaerobic methane oxidation by *Methylopirabilis oxyfera*. *Geochimica  
698 et Cosmochimica Acta* **89**, 256–264.
- 699 Rataj M., Kauth J. and Donnelly M. (1991) Oxidation of deuterated compounds by high specific activity methane  
700 monooxygenase from *Methylosinus trichosporium*. Mechanistic implications. *Journal of Biological  
701 Chemistry* **266**, 18684–18690.
- 702 Reeburgh W. S. (1976) Methane consumption in Cariaco Trench waters and sediments. *Earth and Planetary  
703 Science Letters* **28**, 337–344.
- 704 Reeburgh W. S. (2007) Oceanic methane biogeochemistry. *Chemical Reviews* **107**, 486–513.
- 705 Rees C. (1973) A steady-state model for sulphur isotope fractionation in bacterial reduction processes. *Geochim.  
706 Cosmochim. Acta* **37**, 1141–1162.
- 707 Rigby M., Manning A. and Prinn R. (2012) The value of high-frequency, high-precision methane isotopologue  
708 measurements for source and sink estimation. *Journal of Geophysical Research: Atmospheres (1984–2012)*  
709 **117**.
- 710 Saueressig G., Bergamaschi P., Crowley J., Fischer H. and Harris G. (1995) Carbon kinetic isotope effect in the  
711 reaction of  $\text{CH}_4$  with Cl atoms. *Geophysical Research Letters* **22**, 1225–1228.
- 712 Saueressig G., Bergamaschi P., Crowley J., Fischer H. and Harris G. (1996) D/H kinetic isotope effect in the  
713 reaction  $\text{CH}_4 + \text{Cl}$ . *Geophysical Research Letters* **23**, 3619–3622.
- 714 Saueressig G., Crowley J. N., Bergamaschi P., Brühl C., Brenninkmeijer C. A. and Fischer H. (2001) Carbon 13  
715 and D kinetic isotope effects in the reactions of  $\text{CH}_4$  with O (1 D) and OH: New laboratory measurements  
716 and their implications for the isotopic composition of stratospheric methane. *Journal of Geophysical  
717 Research: Atmospheres (1984–2012)* **106**, 23127–23138.
- 718 Scheller S., Goenrich M., Boecher R., Thauer R. K. and Jaun B. (2010) The key nickel enzyme of methanogenesis  
719 catalyses the anaerobic oxidation of methane. *Nature* **465**, 606–608.
- 720 Sessions A. L. and Hayes J. M. (2005) Calculation of hydrogen isotopic fractionations in biogeochemical  
721 systems. *Geochimica et Cosmochimica Acta* **69**, 593–597.
- 722 Sirajuddin S. and Rosenzweig A. C. (2015) Enzymatic oxidation of methane. *Biochemistry* **54**, 2283–2294.

- 723 Stolper D. A., Lawson M., Davis C. L., Ferreira A. A., Santos Neto E. V., Ellis G. S., Lewan M. D., Martini A.  
724 M., Tang Y., Schoell M., Sessions A. L. and Eiler J. M. (2014a) Formation temperatures of thermogenic and  
725 biogenic methane. *Science* **344**, 1500–1503.
- 726 Stolper D. A., Sessions A. L., Ferreira A. A., Neto E. V. S., Schimmelmann A., Shusta S. S., Valentine D. L. and  
727 Eiler J. M. (2014b) Combined <sup>13</sup>C-D and D-D clumping in methane: methods and preliminary results.  
728 *Geochimica et Cosmochimica Acta* **126**, 169–191.
- 729 Stolper D., Martini A., Clog M., Douglas P., Shusta S., Valentine D., Sessions A. and Eiler J. (2015)  
730 Distinguishing and understanding thermogenic and biogenic sources of methane using multiply substituted  
731 isotopologues. *Geochimica et Cosmochimica Acta* **161**, 219–247.
- 732 Takai K., Nakamura K., Toki T., Tsunogai U., Miyazaki M., Miyazaki J., Hirayama H., Nakagawa S., Nunoura T.  
733 and Horikoshi K. (2008) Cell proliferation at 122 C and isotopically heavy CH<sub>4</sub> production by a  
734 hyperthermophilic methanogen under high-pressure cultivation. *Proceedings of the National Academy of*  
735 *Sciences* **105**, 10949–10954.
- 736 Templeton A. S., Chu K.-H., Alvarez-Cohen L. and Conrad M. E. (2006) Variable carbon isotope fractionation  
737 expressed by aerobic CH<sub>4</sub>-oxidizing bacteria. *Geochimica et Cosmochimica Acta* **70**, 1739–  
738 1752.
- 739 Tyler S. C., Ajie H. O., Rice A. L., Cicerone R. J. and Tuazon E. C. (2000) Experimentally determined kinetic  
740 isotope effects in the reaction of CH<sub>4</sub> with Cl: Implications for atmospheric CH<sub>4</sub>. *Geophysical Research*  
741 *Letters* **27**, 1715–1718.
- 742 Valentine D. L. (2011) Emerging topics in marine methane biogeochemistry. *Annual Review of Marine Science* **3**,  
743 147–171.
- 744 Valentine D. L., Chidthaisong A., Rice A., Reeburgh W. S. and Tyler S. C. (2004) Carbon and hydrogen isotope  
745 fractionation by moderately thermophilic methanogens. *Geochimica et Cosmochimica Acta* **68**, 1571–1590.
- 746 Vavilin V. A., Rytov S. V., Shim N. and Vogt C. (2015) Non-linear dynamics of stable carbon and hydrogen  
747 isotope signatures based on a biological kinetic model of aerobic enzymatic methane oxidation. *Isotopes in*  
748 *environmental and health studies*, 1–18.
- 749 Wahlen M. (1993) The global methane cycle. *Annual Review of Earth and Planetary Sciences* **21**, 407–426.
- 750 Wang D. T., Gruen D. S., Lollar B. S., Hinrichs K.-U., Stewart L. C., Holden J. F., Hristov A. N., Pohlman J. W.,  
751 Morrill P. L., Könneke M., Delwiche K. B., Reeves E. P., Sutcliffe C. N., Ritter D. J., Seewald J. S.,  
752 McIntosh J. C., Hemond H. F., Kubo M. D., Cardace D., Hoehler T. M. and Ono S. (2015) Nonequilibrium  
753 clumped isotope signals in microbial methane. *Science* **348**, 428–431.
- 754 Wang Z., Schauble E. A. and Eiler J. M. (2004) Equilibrium thermodynamics of multiply substituted  
755 isotopologues of molecular gases. *Geochimica et Cosmochimica Acta* **68**, 4779–4797.
- 756 Ward N., Larsen Ø., Sakwa J., Bruseth L., Khouri H., Durkin A. S., Dimitrov G., Jiang L., Scanlan D., Kang K.  
757 H., Lewis M., Nelson K. E., Methé B., Wu M., Heidelberg J. F., Paulsen I. T., Fouts D., Ravel J., Tettelin H.,  
758 Ren Q., Read T., DeBoy R. T., Seshadri R., Salzberg S. L., Jensen H. B., Birkeland N. K., Nelson W. C.,  
759 Dodson R. J., Grindhaug S. H., Holt I., Eidhammer I., Jonassen I., Vanaken S., Utterback T., Feldblyum T. V.,  
760 Fraser C. M., Lillehaug J. R. and Eisen J. A. (2004) Genomic Insights into Methanotrophy: The Complete  
761 Genome Sequence of *Methylococcus capsulatus* (Bath). *PLoS Biol* **2**, e303.

- 762 Welander P. V. and Summons R. E. (2012) Discovery, taxonomic distribution, and phenotypic characterization of  
763 a gene required for 3-methylhopanoid production. *Proceedings of the National Academy of Sciences* **109**,  
764 12905–12910.
- 765 Whitehill A. R., Joelsson L. M. T., Schmidt J. A., Wang D. T., Johnson M. S. and Ono S. Clumped isotope effects  
766 during OH and Cl oxidation of methane. *Geochimica et Cosmochimica Acta* **submitted**.
- 767 Whiticar M. J. (1999) Carbon and hydrogen isotope systematics of bacterial formation and oxidation of methane.  
768 *Chemical Geology* **161**, 291–314.
- 769 Whiticar M. and Schaefer H. (2007) Constraining past global tropospheric methane budgets with carbon and  
770 hydrogen isotope ratios in ice. *Philosophical Transactions of the Royal Society A: Mathematical, Physical*  
771 *and Engineering Sciences* **365**, 1793–1828.
- 772 Whittenbury R., Phillips K. and Wilkinson J. (1970) Enrichment, isolation and some properties of methane-  
773 utilizing bacteria. *Journal of General Microbiology* **61**, 205–218.
- 774 Wilkins P. C., Dalton H., Samuel C. J. and Green J. (1994) Further Evidence for Multiple Pathways in Soluble  
775 Methane-Monooxygenase-Catalysed Oxidations from the Measurement of Deuterium Kinetic Isotope Effects.  
776 *European Journal of Biochemistry* **226**, 555–560.
- 777 Yeung L. Y. (2016) Combinatorial effects on clumped isotopes and their significance in biogeochemistry.  
778 *Geochimica et Cosmochimica Acta* **172**, 22–38.
- 779 Yeung L. Y., Young E. D. and Schauble E. A. (2012) Measurements of  $^{18}\text{O}^{18}\text{O}$  and  $^{17}\text{O}^{18}\text{O}$  in the atmosphere  
780 and the role of isotope-exchange reactions. *Journal of Geophysical Research: Atmospheres (1984–2012)* **117**.
- 781 Yoshinaga M. Y., Holler T., Goldhammer T., Wegener G., Pohlman J. W., Brunner B., Kuypers M. M., Hinrichs  
782 K.-U. and Elvert M. (2014) Carbon isotope equilibration during sulphate-limited anaerobic oxidation of  
783 methane. *Nature Geoscience* **7**, 190–194.
- 784 Young E. D., Rumble D., Freedman P. and Mills M. (2016) A large-radius high-mass-resolution multiple-  
785 collector isotope ratio mass spectrometer for analysis of rare isotopologues of  $\text{O}_2$ ,  $\text{N}_2$ ,  $\text{CH}_4$  and other gases.  
786 *International Journal of Mass Spectrometry* **401**, 1–10.

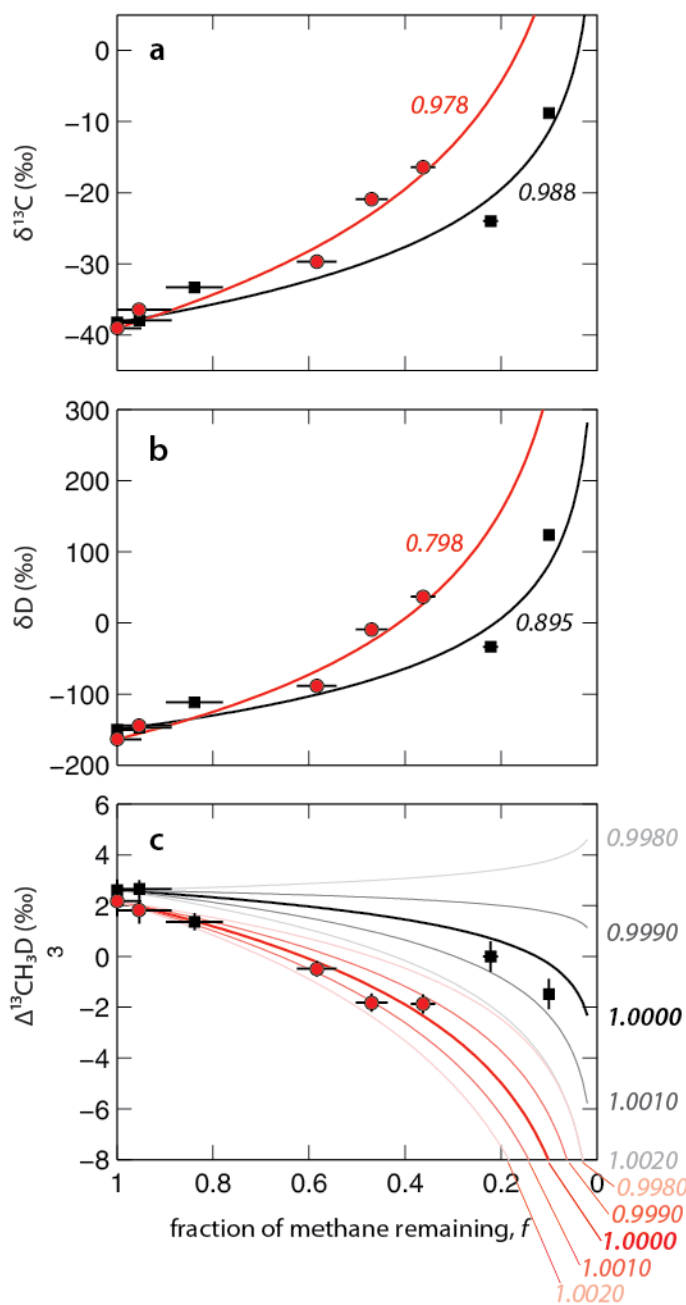
787

788

789

790

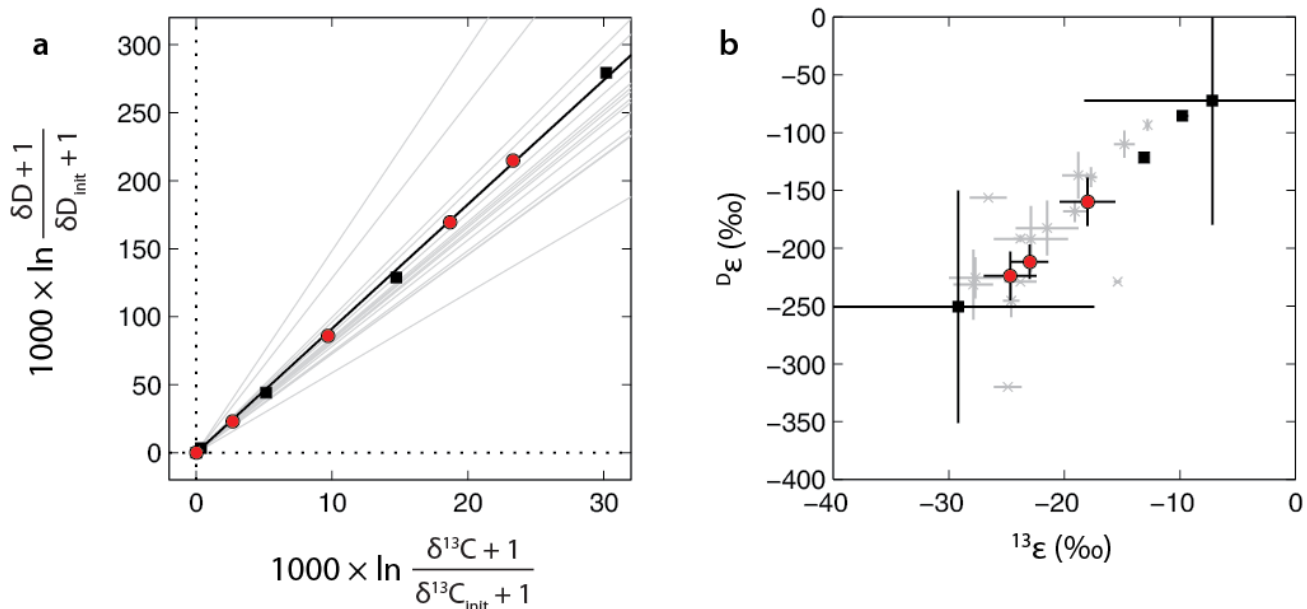
## 8. FIGURES



792

793 Fig. 1. Measured and modeled changes in (a)  $\delta^{13}\text{C}$ , (b)  $\delta\text{D}$ , and (c)  $\Delta^{13}\text{CH}_3\text{D}$  of residual methane as a function of  
 794  $f$ , the fraction of initial methane remaining. Data points from the 30 and 37 °C experiments (Table 1) are shown  
 795 with black and red symbols, respectively. Horizontal error bars represent propagated  $\pm 1\sigma$  uncertainties from GC  
 796 measurements, and vertical error bars represent 95% confidence intervals from isotopologue ratio analyses. Solid  
 797 lines represent the modeled values (from Eqns. 13, 16, and 20) based on the calculated weighted-average carbon-  
 798 and hydrogen-isotope fractionation factors for each set of experiments as listed in Table 1. Labels in *italics*

799 represent  $^{13}\alpha$ ,  $^D\alpha$ , &  $\gamma$ , respectively, in panels (a), (b), & (c). Panel (c) shows model results calculated assuming  
800 different values of  $\gamma$  varying between 0.9980 and 1.0020.

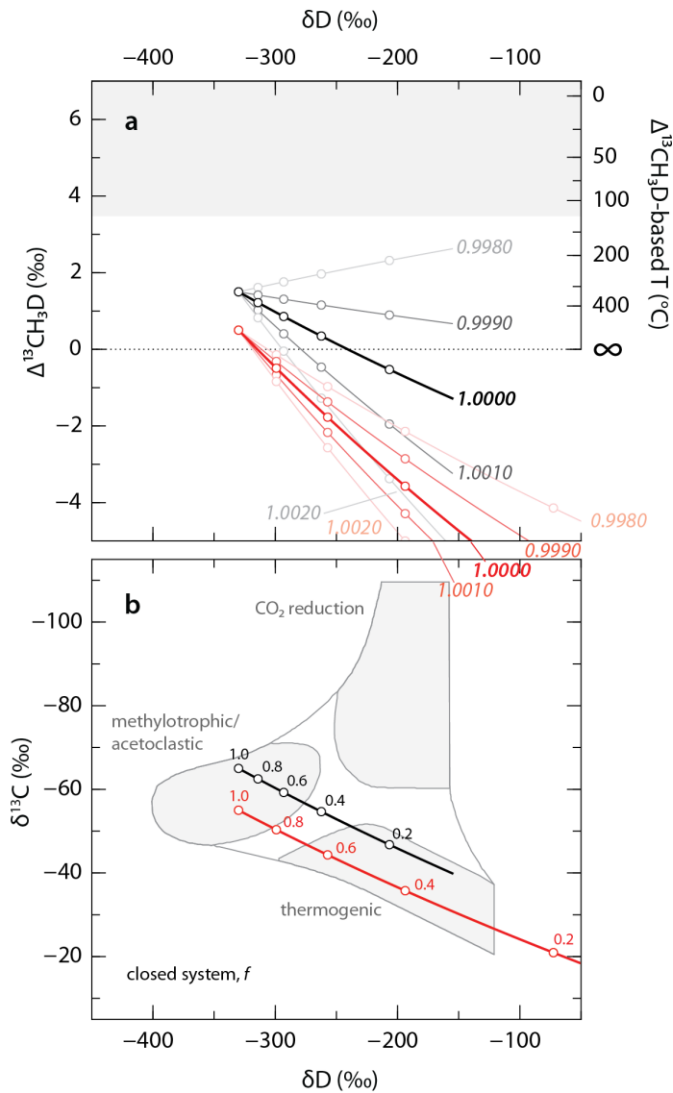


801

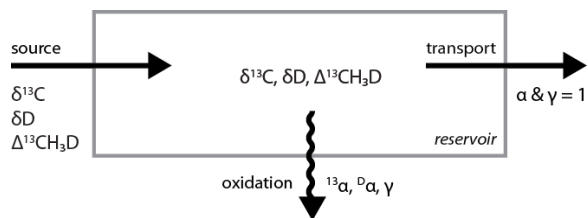
802 Fig. 2. Relationship between fractionation of carbon and hydrogen isotopes. (a) Data from the 30 and 37 °C  
 803 experiments (Table 1) are shown with black and red symbols, respectively. Black line ( $y = 9.14 x$ ) represents the  
 804 best-fit regression through the data. From Eqn. 17, the slope of this line is  $(^{\text{D}}\alpha - 1)/(^{13}\alpha - 1)$ , or  $^{\text{D}}\epsilon/^{13}\epsilon$ . Near the  
 805 origin, the  $x$ - and  $y$ -axes are approximately equal to  $\delta^{13}\text{C} - \delta^{13}\text{C}_{\text{init}}$  and  $\delta\text{D} - \delta\text{D}_{\text{init}}$ , respectively; this  
 806 approximation becomes less accurate with increasing distance from the origin, particularly for hydrogen (Sessions  
 807 and Hayes, 2005). Gray lines represent previously-reported correlations between fractionation of carbon and  
 808 hydrogen isotopes by aerobic methanotrophs determined from experiments with pure cultures (Feisthauer et al.,  
 809 2011) and enrichment cultures (Coleman et al., 1981; Kinnaman et al., 2007; Powelson et al., 2007). (b)  
 810 Fractionation factors ( $\epsilon$ , defined as  $\alpha - 1$ ) calculated for individual bottle incubations from this study (Table 1)  
 811 plotted against fractionation factors reported in the cited studies (gray). One point from the 37 °C experiment (41  
 812 h) was not plotted because of large uncertainties arising from a minimal extent of reaction.

813

814



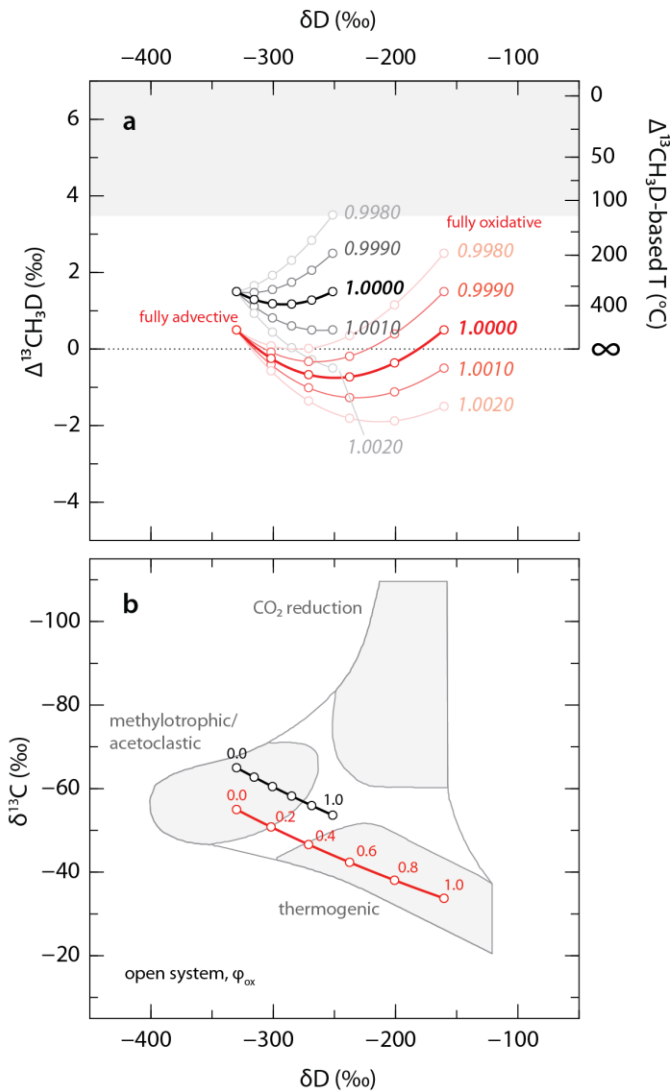
817 Fig. 3. Modeled changes in (a)  $\Delta^{13}\text{CH}_3\text{D}$  vs.  $\delta\text{D}$  and (b)  $\delta^{13}\text{C}$  vs.  $\delta\text{D}$  of residual methane during aerobic methane  
 818 oxidation under closed system conditions. Solid lines represent model predictions (from Eqns. 13, 16, and 20)  
 819 based on the calculated weighted-average carbon- and hydrogen-isotope fractionation factors for each set of  
 820 experiments (black, 30 °C; red, 37 °C) as listed in Table 1 and shown in Fig. 1. Labels in *italics* in panel (a)  
 821 represent  $\gamma$  values. Circles are marked at intervals of 0.2 in  $f$ , the fraction of initial methane remaining, and  
 822 labeled in panel (b). For visual clarity, the models were initialized at slightly different  $\delta^{13}\text{C}$  and  $\Delta^{13}\text{CH}_3\text{D}$  values.  
 823 The initial isotope values were chosen for illustrative purposes only and do not represent any particular natural  
 824 sample; however, the chosen values are typical of modern microbial methane generated in wetland and lake  
 825 sediments. Following Wang et al. (2015), the gray field in panel (a) represents the temperature range within  
 826 which microbial life has been shown to occur (Takai et al., 2008), and the gray fields in panel (b) represent  
 827 empirical methane source fields suggested by Whiticar (1999).



829

830 Fig. 4. Representation of a model open system in which methane is transported in and out via advection, and in  
 831 which aerobic methane oxidation is also occurring. The fractional contribution of oxidation to the total sinks is  
 832  $\phi_{\text{ox}}$ . See Fig. 5 and discussion in Sec. 4.2.1.

833



834

835 Fig. 5. Modeled steady-state values of (a)  $\Delta^{13}\text{CH}_3\text{D}$  vs.  $\delta\text{D}$  and (b)  $\delta^{13}\text{C}$  vs.  $\delta\text{D}$  of methane in an open system  
 836 (Fig. 4) consisting of a single source and two sinks (aerobic methane oxidation and advection). Advection is  
 837 assumed to be non-fractionating. Lines were modeled using Eqns. 22 and 23, and the same fractionation factors  
 838 for aerobic methane oxidation as for those shown with the same line style in Fig. 2. Labels in *italics* in panel (a)  
 839 represent  $\gamma$  values associated with aerobic methane oxidation. Circles are marked at intervals of 0.2 in  $\phi_{\text{ox}}$ , the  
 840 fraction of methane removed via oxidation, ranging from fully advective ( $\phi_{\text{ox}} = 0$ ) to fully oxidative ( $\phi_{\text{ox}} = 1$ ), and  
 841 labeled in panel (b). When  $\phi_{\text{ox}} = 0$ , the isotopic composition of methane in the reservoir is identical to that of the  
 842 source. For visual clarity, the calculations were performed for slightly different  $\delta^{13}\text{C}$  and  $\Delta^{13}\text{CH}_3\text{D}$  values of input  
 843 methane. For description of shaded fields, see the caption for Fig. 3.

844

845

846

## 9. TABLES

847

848 Table 1

849 Experimental results and calculated fractionation factors for batch cultures of *Methylococcus capsulatus* Bath. Uncertainties  
 850 ( $\pm 1\sigma$ ) listed for  $f$ ,  $^{13}\alpha$ ,  $^D\alpha$ , and  $\gamma$  are propagated from those associated with individual measurements according to standard  
 851 formulas (Ku, 1969).

time (h)	$f$	CO <sub>2</sub> (cm <sup>3</sup> ) <sup>a</sup>	$\delta^{13}\text{C}$ (‰) <sup>c</sup>	$\delta\text{D}$ (‰) <sup>c</sup>	$\Delta^{13}\text{CH}_3\text{D}$ (‰) <sup>c</sup>	$^{13}\alpha$	$^D\alpha$	$\gamma$	
30 °C	0	1.00 ± 0.05 <sup>b</sup>	<0.2	-38.27	-150.12	2.61 ± 0.43			
	12	0.95 ± 0.07	0.6	-37.94	-147.20	2.66 ± 0.34	0.993 ± 0.011	0.928 ± 0.107	0.9983 ± 0.0130
	36	0.84 ± 0.06	1.9	-33.31	-111.79	1.36 ± 0.34	0.971 ± 0.012	0.749 ± 0.101	0.9997 ± 0.0060
	- <sup>d</sup>	0.22 ± 0.02	10.3	-24.00	-33.36	-0.01 ± 0.60	0.990 ± 0.0005	0.915 ± 0.004	1.0010 ± 0.0005
	60	0.10 ± 0.01	9.8	-8.81	123.90	-1.48 ± 0.60	0.987 ± 0.0004	0.878 ± 0.004	1.0002 ± 0.0004
						weighted average <sup>e</sup>	0.988 ± 0.0003	0.895 ± 0.003	1.0005 ± 0.0003
37 °C	0	1.00 ± 0.05 <sup>b</sup>	n.d.	-39.06	-163.57	2.17 ± 0.59			
	41	0.95 ± 0.07	n.d.	-36.45	-144.23	1.82 ± 0.53	0.943 ± 0.086	0.516 ± 0.726	0.9585 ± 0.2130
	44	0.58 ± 0.04	2.5	-29.68	-88.51	-0.48 ± 0.30	0.982 ± 0.002	0.840 ± 0.021	1.0025 ± 0.0015
	48	0.47 ± 0.03	4.8	-20.95	-9.20	-1.82 ± 0.36	0.975 ± 0.002	0.776 ± 0.021	0.9997 ± 0.0014
	51	0.36 ± 0.03	6.3	-16.39	36.83	-1.87 ± 0.38	0.977 ± 0.002	0.788 ± 0.015	0.9989 ± 0.0011
						weighted average <sup>e</sup>	0.978 ± 0.001	0.798 ± 0.010	1.0000 ± 0.0007

852

853 n.d., not determined

854

855 <sup>a</sup> Total inorganic carbon in the bottle (including gaseous CO<sub>2</sub> and dissolved inorganic carbon), reported as cm<sup>3</sup>-equivalent of  
 856 CO<sub>2</sub> at standard ambient temperature and pressure (SATP; 25 °C, 1 bar), was estimated from headspace CO<sub>2</sub> concentration  
 857 (determined via GC), the Henry's law constant for CO<sub>2</sub> at room temperature, and the volume of headspace and of HCl-spiked  
 858 medium. Uncertainty is estimated at  $\pm 10\%$ . Quantitative conversion of initial CH<sub>4</sub> (see Sec. 2.1) into CO<sub>2</sub> (i.e., 100%  
 859 oxidation with no incorporation of CH<sub>4</sub>-derived carbon into biomass) would yield 20 cm<sup>3</sup> SATP of CO<sub>2</sub>.

860 <sup>b</sup> An uncertainty of  $\pm 5\%$  was assigned to the initial value of  $f$  to account for variability in starting amounts of methane  
 861 between bottles (see Sec. 2.1). This uncertainty is propagated throughout the calculations for later timepoints.

862 <sup>c</sup> Values for  $\delta^{13}\text{C}$ ,  $\delta\text{D}$ , and  $\Delta^{13}\text{CH}_3\text{D}$  are reported relative to PDB, SMOW, and the stochastic distribution, respectively.  
 863 Uncertainties for  $\delta^{13}\text{C}$ ,  $\delta\text{D}$  (both ca. 0.1‰), and  $\Delta^{13}\text{CH}_3\text{D}$  (listed) are 95% confidence intervals over all cycles in a single  
 864 analysis (see Wang et al., 2015), but are conservatively treated as  $1\sigma$  for purposes of error propagation.

865 <sup>d</sup> Time not recorded.

866 <sup>e</sup> Weighted means of each set of  $^{13}\alpha$ ,  $^D\alpha$ , and  $\gamma$  values, weighted by  $1/\sigma^2$ . Uncertainty ( $1\sigma$ ) in weighted means was estimated  
 867 following Bevington and Robinson (2002).

868

869 Table 2

870 Comparison of experimentally-determined ratios of carbon- and hydrogen-isotope fractionation factors ( $^{13}\epsilon$ ) and  $^{13}\text{CH}_3\text{D}$   
 871 fractionation factors ( $\gamma$ ) for different methane sink processes. Uncertainties quoted are  $\pm 2\sigma$  or 95% confidence interval.

	$^{13}\epsilon$	$\gamma$
<i>Aerobic methane oxidation</i>		
Previous work <sup>a</sup>	5.9 to 14.9	
This study <sup>b</sup>	9.14 $\pm$ 0.14	1.0004 $\pm$ 0.0006
<i>Anaerobic oxidation of methane (AOM)</i>		
Holler et al. (2009)	6.4 to 8.5	
<i>Nitrite-dependent anaerobic methane oxidation</i>		
Rasigraf et al. (2012)	7.8 $\pm$ 0.8	
<i>CH<sub>4</sub> + OH</i>		
Saueressig et al. (2001)	58.5 $\pm$ 6.6	
Joelsson et al. (2014)		0.980 $\pm$ 0.038
Whitehill et al. (in revision)	41.3 $\pm$ 8.3	0.9997 $\pm$ 0.0012
<i>CH<sub>4</sub> + Cl</i>		
Tyler et al. (2000)	5.51	
Saueressig et al. (1995; 1996)	5.50	
Feilberg et al. (2005)	5.65	
Joelsson et al. (2015)		0.978 $\pm$ 0.051
Whitehill et al. (in revision)	5.56	0.9965 $\pm$ 0.0007

872

873 <sup>a</sup> See caption of Fig. 2a for references. Also see Rasigraf et al. (2012) for a compilation of  $^{13}\epsilon$  and  $^{13}\text{CH}_3\text{D}$  values determined for  
 874 biological methane oxidation in cultures and in the environment.

875 <sup>b</sup> Derived from linear regression ( $^{13}\epsilon$ , Fig. 2a) or weighted average ( $\gamma$ ) of all timepoints in both experiments in Table 1.

876

1 Supplementary Data for:

2 Fractionation of the methane isotopologues  $^{13}\text{CH}_4$ ,  $^{12}\text{CH}_3\text{D}$ , and  $^{13}\text{CH}_3\text{D}$  during aerobic oxidation of methane by  
3 *Methylococcus capsulatus* (Bath)

4

5 Authors and affiliations:

6 David T. Wang<sup>a,b,\*</sup>, Paula V. Welander<sup>c</sup>, and Shuhei Ono<sup>a</sup>

7 <sup>a</sup>Department of Earth, Atmospheric and Planetary Sciences, Massachusetts Institute of Technology, Cambridge, Massachusetts 02139, USA.

8 <sup>b</sup>Marine Chemistry and Geochemistry Department, Woods Hole Oceanographic Institution, Woods Hole, Massachusetts 02543, USA.

9 <sup>c</sup>Earth System Science Department, Stanford University, Stanford, California 94305, USA.

10

11 \* To whom correspondence should be addressed:

12 David T. Wang

13 Department of Earth, Atmospheric, and Planetary Sciences

14 Massachusetts Institute of Technology

15 77 Massachusetts Ave, Bldg. E25-645, Cambridge, MA 02139, USA.

16 +1 (617) 324-3949

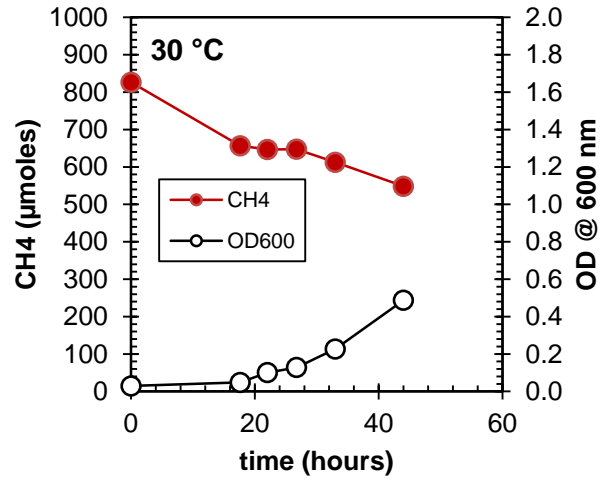
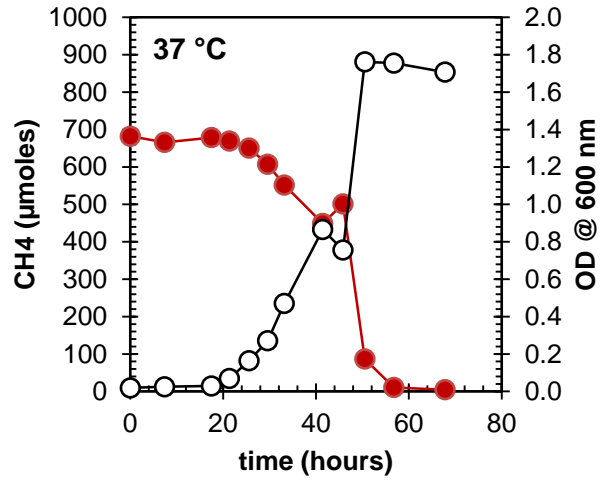
17 [dtw@mit.edu](mailto:dtw@mit.edu)

18

19

20

21



22

23 Supplementary Fig. 1. Measured CH<sub>4</sub> concentrations and optical densities (OD) during preliminary experiments  
 24 at 37 °C (left) and 30 °C (right) with starter cultures of *M. capsulatus* (Bath).